

Binder-Free MOF-Based and MOF-Derived Nanoarrays for Flexible Electrochemical Energy Storage: Progress and Perspectives

Dongming Cai, Zhuxian Yang, Rui Tong, Haiming Huang, Chuankun Zhang, and Yongde Xia*

The fast development of Internet of Things and the rapid advent of next-generation versatile wearable electronics require cost-effective and highly-efficient electroactive materials for flexible electrochemical energy storage devices. Among various electroactive materials, binder-free nanostructured arrays have attracted widespread attention. Featured with growing on a conductive and flexible substrate without using inactive and insulating binders, binder-free 3D nanoarray electrodes facilitate fast electron/ion transportation and rapid reaction kinetics with more exposed active sites, maintain structure integrity of electrodes even under bending or twisted conditions, readily release generated joule heat during charge/discharge cycles and achieve enhanced gravimetric capacity of the whole device. Binder-free metal-organic framework (MOF) nanoarrays and/or MOF-derived nanoarrays with high surface area and unique porous structure have emerged with great potential in energy storage field and been extensively exploited in recent years. In this review, common substrates used for binder-free nanoarrays are compared and discussed. Various MOF-based and MOF-derived nanoarrays, including metal oxides, sulfides, selenides, nitrides, phosphides and nitrogen-doped carbons, are surveyed and their electrochemical performance along with their applications in flexible energy storage are analyzed and overviewed. In addition, key technical issues and outlooks on future development of MOF-based and MOF-derived nanoarrays toward flexible energy storage are also offered.

pollution and climate issues, such as global warming and extreme weather conditions. It is therefore urgent and highly desirable to develop renewable and clean energies.^[1,2] Sustainable electrochemical energy storage systems, including supercapacitors, Li/Na/K ion batteries, Li-S batteries, Zn/Air, Zn ion batteries etc., have drawn much attention in recent decades.^[3–8] Moreover, in order to meet mankind's diversified energy needs, the design and realization of novel materials with unique structure and enhanced performance has attracted huge research interests recently.^[9] At present, however, most of the as-obtained flexible energy storage devices are still facing the challenges including unsatisfactory energy efficiencies, low capacity, large overpotential and poor charge–discharge stabilities, mainly due to the sluggish electrochemical reactions. The use of insulated and inactive binders during the electrode fabrication process are one of the key factors accounting for the sluggish electrochemical reactions. Moreover, the binders and conductive additive materials can also reduce the gravimetric capacity of the whole cell system.^[10] To tackle these issues, binder-free electrode


materials, most of which are in-situ grown on a conductive substrate, have emerged as effective alternatives to overcome the inherent barriers of conventional electrode materials and have been fast developed.^[11] In particular, 3D nanoarray structured

1. Introduction

The continuous growing of population and exponential consumption of fossil fuels has led to energy crisis, environmental

D. Cai, R. Tong, H. Huang, C. Zhang
Hubei Key Laboratory of Energy Storage and Power Battery
School of Mathematics
Physics and Optoelectronics Engineering
Hubei University of Automotive Technology
Shiyan 442002, P. R. China

Z. Yang, Y. Xia
Department of Engineering
Faculty of Environment
Science and Economy
University of Exeter
Exeter EX4 4QF, UK
E-mail: Y.Xia@exeter.ac.uk

 The ORCID identification number(s) for the author(s) of this article can be found under <https://doi.org/10.1002/smll.202305778>

© 2023 The Authors. Small published by Wiley-VCH GmbH. This is an open access article under the terms of the Creative Commons Attribution License, which permits use, distribution and reproduction in any medium, provided the original work is properly cited.

DOI: 10.1002/smll.202305778

electrode materials with large surface area and good structural integrity, have been widely explored, which exhibit overwhelming merits compared to their counterparts made from powder materials. First of all, nanoarray structured materials are usually intimately anchored on a substrate, which avoid the use of non-active binders and consequently improve the specific gravimetric capacity of the whole electrode. Second, 3D nanoarray structured materials with relatively ordered architecture can enable the full contact between the active materials and the electrolyte, which can facilitate rapid electron transportation as well as fast ion diffusion, hence enhance the kinetics of the electrodes. Third, binder-free arrayed materials with separated structure can help maintain structural integrity when the electrode is in bent or twisted state, offering strong superiority in flexible energy storage area. Last but not least, 3D nanoarray structured electrodes offer sufficient space to accommodate the volume change and joule heat release during the electrochemical reaction process, achieving long life span and high performance of the devices. These advantages of 3D arrayed electrodes make them promising electroactive materials toward flexible energy storage applications with extensive investigations.^[12,13]

Metal-organic frameworks (MOFs), a typical class of porous crystalline materials assembled from metal ions/clusters with organic ligands via coordination interactions, have been widely investigated.^[14–17] Due to the large number of metal ions and organic ligands, a great diversity of MOFs with adjustable pore sizes and morphologies have been developed, which have attracted significant attention in many fields, such as catalysis, gas storage and separation, drug delivery, sensors, energy conversion and storage etc.^[18–28] Most of MOF-based or MOF-derived active materials are produced in form of powder. As a result, in order for them to be used as electrodes in electrochemical applications, polymer binders and additives are needed to fabricate the electrodes, which will inevitably increase the “dead mass” of the electrodes, decrease the electrical conductivity and limit the gravimetric/volumetric capacity of the whole device, thus adversely affect the electron transmission.^[29] These problems can be avoided via the utilization of nanoarray structures. When MOFs are prepared in form of nanoarray on a conductive substrate or deposited on the surface of nanoarrays, the obtained composites not only possess the above-mentioned merits of nanoarrays, but also can fully utilize the high porosity of MOFs. Moreover, the MOF-based nanoarrays can be subjected to heat treatment in controlled atmosphere to form a variety of MOF-derived nanoarrays that are promising and highly sought-after materials for electrochemical energy storage and conversion applications. Consequently, many kinds of MOF-based or MOF-derived nanoarrays have been developed and widely exploited in the field of energy storage.

Driven by the needs of portable electronics and medical devices, electric vehicles, electric grids and the emerging of Internet of Things, flexible electrical energy storage devices which dominantly provide power to various wearable devices currently, hold great potential for numerous practical applications and they may revolutionize the personalized electronics, health care and global supply chains remarkably.^[30] The last decade has witnessed great research interest in wearable technologies which have been rapidly developed and utilized in portable and flexible electronics, such as roll-up displays,

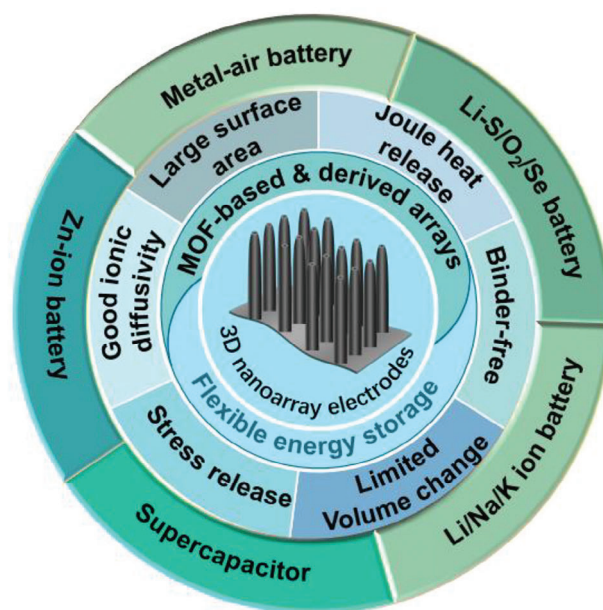


Figure 1. A conceptual overview on binder-free MOF-based and MOF-derived nanoarrays as advanced electrodes for flexible electrochemical energy storage applications.

curved smartphones, as well as plenty of relevant flexible, wearable and portable electronic devices. Many different high performance energy storage devices with excellent flexibility, including Li/Na/K-ions batteries, Li-S batteries, Metal-air batteries, Zn-ions batteries, Supercapacitors, etc. have been exploited. Particularly, various binder-free nanostructured MOF-based and MOF derived nanoarrays as advanced electrodes in flexible electrochemical energy storage applications have been demonstrated (Figure 1).

However, there is still a long way to go to realize commercial application of binder-free nanostructured nanoarrays. To practically use them in flexible electrochemical energy storage devices, the substrate needs to be cost-effective and possesses good conductivity, high electrochemical stability and thermal stability, as well as good elasticity; while the active materials are expected to have high electrochemical capacity, long cycling stability and good adhesion to the substrate. For whole flexible devices, they should not only be easy to prepare in a large scale, but also exhibit high energy density, high power density, good safety and even good elasticity. The research directions and targeted goals of binder-free nanostructured nanoarrays for flexible energy storage are summarized in Figure 2.

So far, there have been many reviews on MOF-based or MOF-derived nanomaterials in electrochemical energy storage and conversion applications, including but not limited to the synthesis, the properties and their utilizations.^[31–39] There are also a couple of reviews that summarized the merits of nanoarray structured materials.^[40,41] However, there has been no systematic overview on the applications of MOF related nanoarray materials in flexible energy storage. So, to bridge this gap, the recent progress on binder-free MOF-based and MOF-derived nanoarrays in flexible energy storage is comprehensively

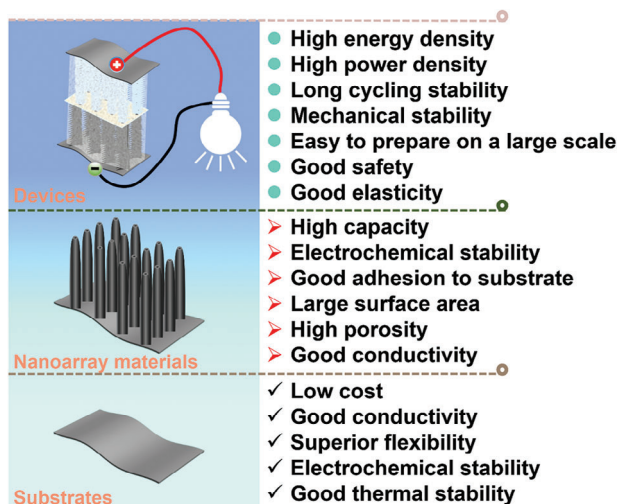


Figure 2. Research directions of binder-free nanostructured nanoarrays for flexible energy storage.

surveyed and summarized in this work. We first overview the commonly used flexible substrates and their advantages and disadvantages. Then we discuss the applications of various nanoarrays scaffold loaded with MOFs/MOF-derived composites or nanoarrays directly made from MOFs/MOF derivatives in detail, including metal oxides, sulfides, selenides, nitrides, phosphides and nitrogen doped carbons, as electrodes in flexible energy storage. Finally, we provide the challenges and outlooks of binder-free nanostructured MOF-based and MOF-derived nanoarrays in flexible energy storage. This review is anticipated to inspire further studies and new ideas on the design and application of unique and novel MOF and MOF-derived nanoarray structured materials in relevant flexible energy storage field.

2. Flexible Substrates for Nanoarray Fabrication

Self-supported nanoarray structures without polymer binder in electrodes can effectively reduce the risk of potential blockage of active sites, maintain the morphology of nanoarrays to enhance the accessibility of electrolyte, and accordingly improve the long-term stability of the electrodes. To achieve flexible energy storage, the use of an appropriate substrate is crucial. Typically, the fabricated flexible electrodes require the substrates to possess good conductivity, high porosity, large specific surface area, considerable mechanical flexibility, etc. The key factors of some commonly used flexible substrates are shown and compared in **Figure 3**. Representative substrates for flexible electrodes are briefly reviewed in this section.

2.1. Carbon Cloth

Carbon cloth (CC), a very common commercially available substrate which is made from uniform carbon fibers, has been widely used as substrate in flexible energy storage field due to

its excellent electric conductivity, high thermal stability and comparable mechanical flexibility.^[42–44] For example, various kinds of active materials, such as Fe_2O_3 ,^[45,46] FeOOH ,^[47,48] MnO_2 ,^[49] MoO_3 ,^[50,51] NiCo_2O_4 ,^[52] VN ^[53] etc., have been successfully anchored on CC as flexible energy storage electrodes. However, the inherent hydrophobicity, intrinsically small specific surface area ($\approx 5 \text{ m}^2 \text{ g}^{-1}$) and high price of CC limit its practical applications in a large scale. In order to modify the hydrophilicity of CC, usually strong oxidant or concentrated acid is required. Due to the poor electrochemical reactivity and low accessible surface area, CC is rarely directly used as active electrode. However, some studies were devoted to modify the pristine CC in order to fully release the charge storage capability of CC.^[54–56] At present, the widely adopted methods to boost the capacitances of CCs include nanostructure fabrication and doping with nonmetal elements. While the nanostructure fabrication method can increase the porosity and/or specific surface area of the CC, thereby provides faster ion diffusion and enhanced electrochemical capacitance, the non-metal element doping can effectively adjust the electron structure and improves the conductivity as well as the hydrophilicity of the electroactive material, and therefore introduce redox reaction and extra electrochemical capacitance. For example, Qin et al. prepared Na-CC by one-step electrochemical reduction in aqueous Na_2SO_4 solution,^[57] in which Na^+ was introduced into the surface of CC, consequently the resulting Na-CC prevented the adsorption of H^+ and expands the work potential window of the anode. Moreover, Han et al. successfully fabricate activated porous CC with oxygen-containing functional groups by a chemical etching plus electrochemical activation method.^[58] By virtue of such a favorable characteristic, the prepared activated porous CC exhibited remarkable surface area of $201.3 \text{ m}^2 \text{ g}^{-1}$ and excellent electrochemical capacitance of 1.2 F cm^{-2} at 4 mA cm^{-2} . In the future, if CC can be produced more cheaply without altering the physical and chemical properties, the large-scale development of flexible energy storage devices based on CC substrate will be very promising.

2.2. Electrospun Nanofiber

In recent decades, electrospinning technique has been applied in the preparation of nanofiber materials for flexible energy storage. The high surface area and excellent surface-to-volume ratio can offer numerous active sites and controllable porous structures, which can buffer the huge volume changes during battery cycling and boost the infiltration of electrolytes.^[59–64] Moreover, electrospun nanofiber mats also possess favorable properties for flexible electrochemical electrodes, including desirable mechanical strength, easily adjustable chemical compositions (as the additives of electrospinning solution can range from organic polymers to inorganic compounds), and tunable diameters of nanofiber, which are generally controlled by the working voltages, the distances between the needle tip and the stationary plate, the feeding rates electrospinning solution and the fiber deposition rates.

On account of the above merits, electrospun nanofibers have been extensively exploited as promising flexible electrode substrates for various energy storage applications.^[65–68] For instance, Poudel et al. reported the use of hollow porous carbon nanofibers

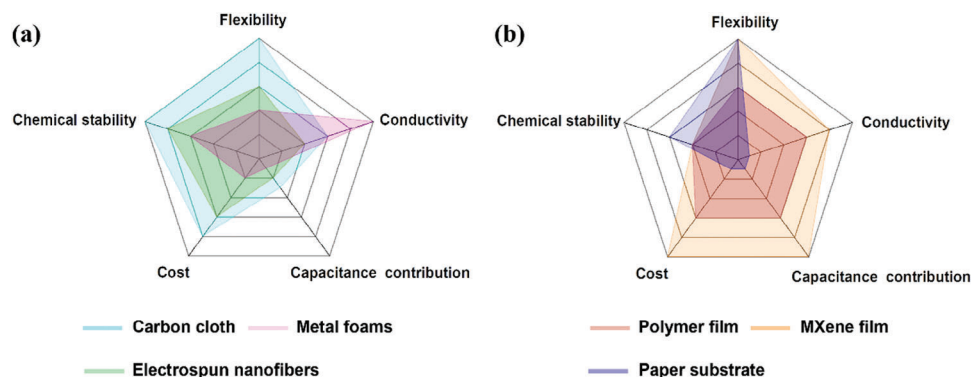


Figure 3. a,b) Multiangle comparison of some common substrates used in flexible energy storage field.

(CNF) as current collector in supercapacitor, which was prepared by coaxial electrospinning followed by carbonization.^[69] Ji et al. produced polyacrylonitrile (PAN) electrospun nanofibers as current collector for Zn-air battery cathode,^[60] in which MOF derived Co single atom particles were anchored in the carbon nanoflakes. Moreover, Yao et al. demonstrated the use of ZIF-67 and PAN to prepare electrospun film and then calcinated it with melamine to obtain Co-containing CNTs (Co-C@CNF-CNT) substrate. After further sulfurization of the substrate, the flexible Co-S@CNF-CNT electrode can be readily obtained.^[70] The versatile electrospun fibers can be used not only as current collector/ substrate, but also as separator or free-standing electrode.

Recently, Liu et al. reported the preparation of synchronous-ultrahigh conductive and reactive N-atom doped flexible carbon nanofiber networks (SH-FCNNs) as free-standing electrode for supercapacitor.^[71] The porous PAN was first prepared by washing the as-synthesized electrospun PAN/PVP nanofibers with deionized water to dissolve the polyvinylpyrrolidone (PVP), then polyaniline (PANI) nanowires were implanted on the porous PAN by an in-situ polymerization reaction, which was further pre-oxidized and calcined to get SH-FCNNs. The as-obtained SH-FCNNs electrode achieved capacitance of 580.9 F g^{-1} at 0.5 A g^{-1} in $1 \text{ M H}_2\text{SO}_4$ electrolyte solution and exhibited superior electrochemical stability and flexibility. Interestingly, when a layer of PANI was electrodeposited on SH-FCNNs, the Zn-SH-FCNNs@PANI composite was also an ideal cathode material for flexible aqueous Zn ion batteries. Moreover, Kim et al. demonstrated that well-defined 1D hollow carbon fiber with lithiophilic Au nanoparticles could be fabricated through a dual-nozzle electrospinning technique, and the resulting material can be used as Li host for Li-ion batteries.^[72] In addition, Yan et al. also directly used pre-stabilized PAN mat as separator to assemble flexible Mn/Fe asymmetric supercapacitor with negative Poisson's ratio structure.^[73]

The preparation of a uniform nanofiber film with good flexibility is usually not as easy as expected, since many factors, such as environmental temperature, humidity, viscosity and conductivity of electrospinning solution, electrospinning operation voltage, etc., can inevitably affect the quality of the synthesized nanofiber film. In addition, nanofiber film often cannot be directly used unless it has been treated at high temperatures. After heat treatment, the resulting film with en-

hanced conductivity is often compromised by its mechanical flexibility.

2.3. Paper-Based Materials

Apart from electrospinning nanofiber mats, paper-based materials for flexible energy storage devices have also been widely explored due to their low cost, high flexibility and environmental friendliness.^[74–77] The rough surface and high porosity nature of paper enable fast ion transport, and the simple manufacture technique of paper makes it promising for large scale fabrication. However, the poor conductivity of some paper inevitably restricts the utilization of paper-based energy storage devices. Many attempts have been therefore devoted to solving this problem. For example, Zheng et al. drew graphite on cellulose paper simply by a pencil to increase the conductivity of paper based electrode.^[78] Liu et al. directly coated graphene on commercial paper to obtain highly conductive flexible paper substrate and then electrodeposited polyaniline nanorods on it that was used as electrode for flexible supercapacitor.^[79] The use of green electrochemical oxidation/exfoliation technique to modify graphite paper (GP) was demonstrated by Mandal et al.^[80] This method not only increased the specific surface area of GP, but also enhanced its capacitance and charge storage kinetics. Zhang et al. also applied electroless deposition of Ni on a laboratory filter paper to enhance its electrical conductivity, which was directly used as substrate to load active materials as flexible electrode for supercapacitor.^[81]

Moreover, some researchers attempted to utilize home-made conductive paper substrates to overcome the poor electrical conductivity of pristine paper-based electrode. For instance, Wu et al. fabricated bacterial cellulose embedded cellulosic fiber matrix paper with high conductivity up to $5.9 \times 10^{-1} \text{ S cm}^{-1}$.^[82] Bharti et al. reported the preparation of conductive carbon nanotube (CNT) paper by filtering well dispersed multi-walled CNTs through a vacuum filtration system.^[83] Yang et al. also demonstrated the produced black phosphorus (BP)/CNT composite paper through a vacuum filtration of mixture of well dispersed BP/CNT ink.^[84] The as-obtained BP/CNTs paper exhibited high volume capacitance and outstanding mechanical flexibility. However, the high price of CNT may limit its large-scale utilization.

In addition, the use of recently emerged screen-printing and inkjet-printing techniques for paper can also produce paper-based substrates to fabricate flexible energy storage devices.^[85,86] For example, Sundriyal et al. reported the preparation of a flexible electrode with good conductivity by inkjet-printing graphene oxide (GO) ink on an A4 paper.^[87] The designed conducting patterns on paper was used as flexible substrate for further printing of GO-MnO₂ and active carbon.

2.4. Other Materials

Recently, the use of other materials, such as polymers, for the fabrication of flexible conductive films as alternatives of CC and electrospun fibers, have drawn increased attention due to the high cost of CC and the poor conductivity of electrospun film. Polymer-based substrates possess good elastic, excellent mechanical flexibility and moderate chemical stability.^[10,88–90] For example, free-standing polypyrrole (PPy) membranes with high surface/mass ratio, good mechanical flexibility, high electrical conductivity and satisfactory capacitance have shown great advantages in flexible energy storage field.^[91] Hou et al. found that free-standing PPy membrane could be used as flexible substrate for supercapacitors,^[92] and the as-obtained single PPy membrane exhibited a low charge transfer resistance of 0.3 Ω cm⁻¹, indicating a fast charge transfer. Moreover, Yue et al. also demonstrated that porous PPy scaffold could be adopted as substrate to grow conductive Cu-CAT MOF, which could be used as electrode in flexible energy storage.^[93]

Apart from polymer films, the newly emerged 2D inorganic compound MXene materials have also been synthesized in film form and were applied in supercapacitors and batteries. The layered structure, extraordinary conductivity (≈8700 S cm⁻¹) as well as certain capacitance contribution make MXene a popular material and a rising star in the family of 2D materials.^[94,95] For instance, Wang et al. directly filtered MXene solution to prepare free-standing MXene electrode for flexible supercapacitor.^[96] The synthesized free-standing MXene film showed a specific capacitance up to 400 F g⁻¹; when the as-prepared free-standing MXene film was matched with free-standing MnO₂-CNT cathode, the assembled aqueous Zn-ion capacitor exhibited an energy density of 98.6 Wh kg⁻¹. Moreover, Gund et al. also reported the use of MXene/polymer hybrid materials for flexible alternating current filtering capacitor.^[97] Due to the synergistic effect of MXene and polymer, the MXene/polymer composite achieved a high capacitance of 0.56 mF cm⁻² and maintained at a rate up to 1000 V s⁻¹. In addition, the as-assembled device exhibited superb flexibility and excellent cycling stability.

Metal substrates, such as Cu, Al, Pt, Ti, Ni, Au, stainless steel, etc., are also widely used in electrochemical energy storage and conversion as current collectors, substrates or even active materials. Notably, metal foams possess superior electrical conductivity, low cost and good malleability, but have poor flexibility and corrosion resistance. For example, metal foam substrates are often subject to solution or high-temperature thermal treatment to load active materials, which will inevitably introduce impurities due to phase transitions or oxidation state alteration, thus affect the mechanical flexibility of the electrodes. When loading the active materials mass on the metal foam substrates, the formed impu-

rities are often not considered, which will unavoidably affect the overall electrochemical performance significantly.^[98]

2.5. Summary

The use of an appropriate flexible substrate is important and prerequisite in the preparation of flexible nanoarray structures for flexible energy storage. An ideal flexible substrate for future energy storage system requires good electronic conductivity, superior flexibility, low cost and environmental friendliness. The developing of lighter and thinner current collectors with excellent mechanical stability is also highly sought-after and a major trend in this area.^[99]

3. MOF-Based Nanoarrays

Plenty of MOFs have been synthesized due to the numerous selectable ligands and many kinds of metal ions. Pure MOF-based nanoarrays can be prepared through rational design and precise synthesis. Moreover, exploitation of the direct use of conductive MOFs as electrode materials for flexible energy storage can remarkably simplify the preparation process of the electrodes. However, most pristine MOFs lack of electrical conductivity, which inevitably limit their direct applications in energy storage field. Hence, designing and preparing MOFs with good electronic conductivity are of great importance.

Sheberla et al. reported the use of Ni₃(2,3,6,7,10,11-hexaiminotriphenylene)₂ (Ni₃(HITP)₂), a MOF with high electrical conductivity as the sole electrode material in an electrochemical double layer capacitor,^[100] which is the first example of a supercapacitor made entirely from neat MOFs as active materials, without using any conductive additives or other binders. Comparable to the commercial devices, this MOF-based device exhibited an areal capacitance exceeds those of most carbon-based materials with capacity retention greater than 90% over 10 000 charging and discharging cycles. Feng et al. prepared a robust and conductive hexaaminobenzene (HAB)-derived 2D MOF with exceptionally high volumetric and areal capacitance.^[101] As HAB exhibited a strong orbital interaction with Ni(ii)/Cu(ii), the coordination bonds were highly robust against other reactive chemical species. Consequently, both Ni-HAB and Cu-HAB MOFs demonstrated good chemical stabilities in both acidic and basic aqueous environments. Impressively, the HAB-based MOF electrodes exhibited high volumetric capacitances up to 760 F cm⁻³ and good cycling stability with a capacitance retention of 90% even after 12 000 charging/discharging cycles.

Moreover, it is highly desirable to attach MOF material to current collector through chemical bonding, which can achieve better mechanical properties. Li et al. reported the preparation of a conductive MOF (Cu-CAT) nanowire arrays (NWAs) grown on carbon fiber paper, which was used as the sole electrode material for solid-state supercapacitors.^[102] As shown in **Figure 4a1**, Cu ions coordinate to 2, 3, 6, 7, 10, 11-hexahydroxytriphenylene (HHTP) ligands in ab plane to construct a 2D hexagonal lattice, which further packs along the c-axis with a slipped-parallel ab stacking model to form a honeycomb-like porous structure. The formed Cu-CAT has 1D channels along the c-axis with

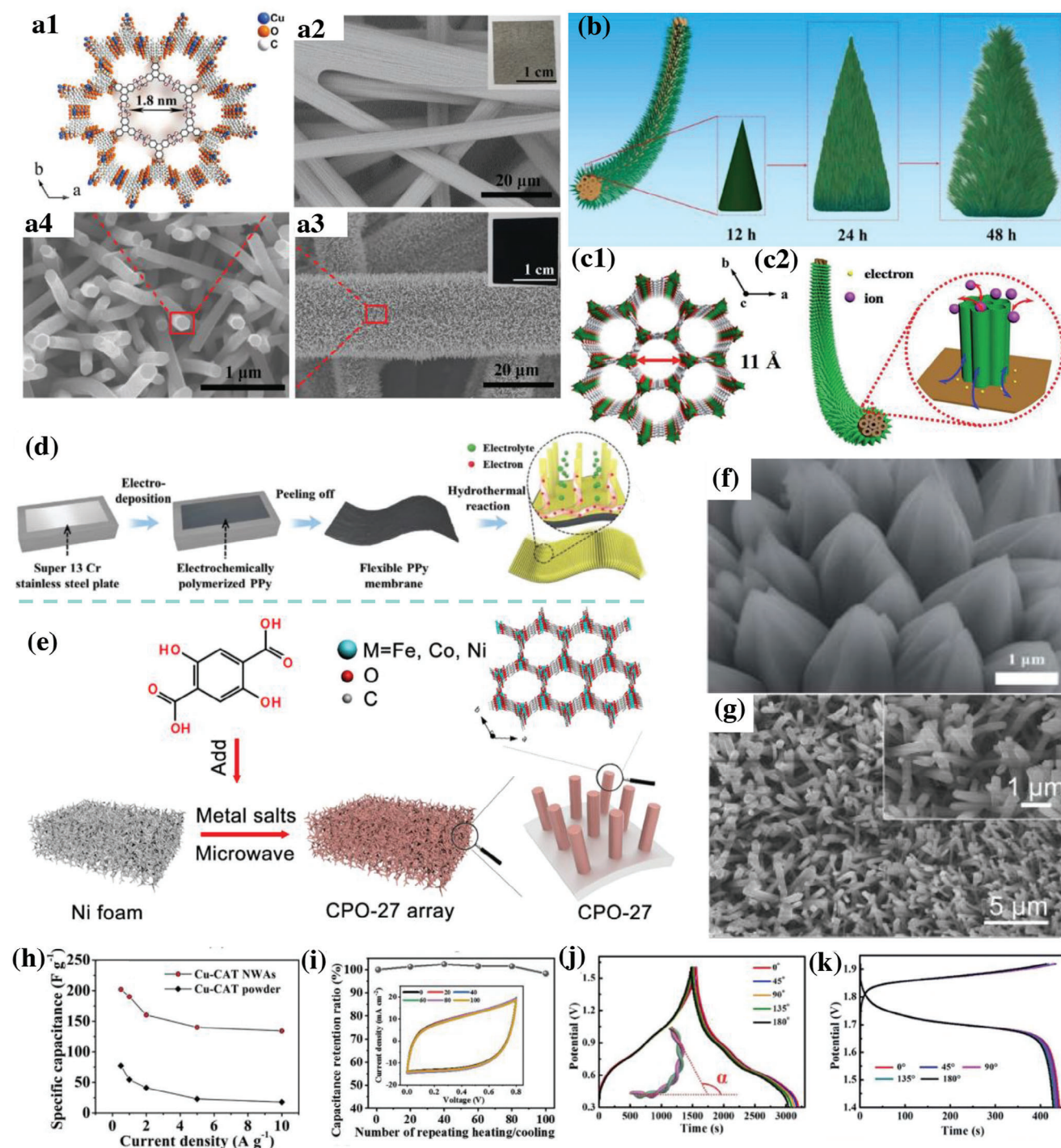


Figure 4. a1) Crystal structure of Cu-CAT viewed along the c-axis. a2) SEM and photomicrographic images (inset in a3) of the carbon fiber paper. a3,a4) SEM and photomicrographic images (inset in a3) of the Cu-CAT NWAs grown on carbon fiber paper. b) Schematic illustration of the preparation process of V-MOF@CNTF with hierarchical nanowire structure. c1) Crystal structure of Ni-MOF-74. c2) Illustration of the electron and ion transportation process of Ni-MOF-74@CNTF. d) Schematic illustration of the preparation process of Cu-CAT-NWAs/PPy. e) Schematic illustration of the preparation process of CPO-27 arrays. The crystal structure of the CPO-27 nanorod is viewed approximately along the (001) direction. H atoms are omitted for clarity. f) SEM images of Ni-MOF-74@CNTF. g) SEM images of CPO-27 grown on the Ni foam substrate annealed at 250°C (CPO-27@250). h) Rate-dependent specific capacitance of Cu-CAT NWAs and Cu-CAT powder. i) CV curves and capacitance retention ratio of Cu-CAT-NWAs/PPy based supercapacitor recorded at different cyclic numbers of repeated heating/cooling. j) GCD curves of the all-solid-state fiber-shaped V-MOF-48//Zn battery at a current density of 0.2 A cm⁻³ under various bending angles. (k) GCD curves at different bending angles of the fiber-shaped quasi-solid-state Ni-MOF-74//Zn battery. a,h) Reproduced with permission.^[102] Copyright 2017, Wiley-VCH. b,j) Reproduced with permission.^[103] Copyright 2019, Elsevier. c,f,k) Reproduced with permission.^[104] Copyright 2019, Royal Society of Chemistry. d,i) Reproduced with permission.^[92] Copyright 2019, Wiley-VCH. e.g) Reproduced with permission.^[109] Copyright 2019, Elsevier.

an open-window size of ≈ 1.8 nm. In the SEM images shown in Figure 4a2–4, blank carbon fibers with smooth surface can be observed, but they are homogeneously covered with high-density oriented nanowires after the growth of Cu-CAT. Due to the nanowire array structure, high porosity and excellent conductivity, the MOF Cu-CAT integrated NWA electrode exhibited a specific capacitance of 202 F g^{-1} at a current density of 0.5 A g^{-1} . When the current density was increased by 20 times, up to 66% of its specific capacitance was remained (Figure 4h). For comparison, Cu-CAT powder electrode only showed half of the capacitance of Cu-CAT NWAs electrode, and retained $\approx 33\%$ of its capacitance when the current density was increased from 0.5 to 10 A g^{-1} .

Although conductive carbon fiber paper (CFP) was used as substrate to anchor MOF Cu-CAT NWAs, it did not contribute to the capacitance, but inevitably introduced inactive component with extra mass to the electrode unit. Moreover, the rigid structure of CFP has poor mechanical flexibility. Thus, Hou et al. addressed this issue by substituting CFP with conductive and flexible polypyrrole (PPy) membrane.^[92] The fabrication procedure and architecture design of the Cu-CAT-NWAs/PPy electrode were schematically shown in Figure 4d. First, PPy membrane was synthesized by constant galvanic electrodeposition approach. Then Cu-CAT-NWAs were directly grown onto the PPy membrane via a facile hydrothermal method. The flexibility and efficient charge transfer property of PPy membrane render it a unique supporting backbone and current collector for the formation of Cu-CAT-NWAs as an integrated flexible electrode. A symmetric all-solid-state flexible supercapacitor was assembled by employing Cu-CAT-NWAs/PPy as both electrodes. As shown in Figure 4i, after 100 alternate heating ($100 \text{ }^\circ\text{C}$)/freezing ($-20 \text{ }^\circ\text{C}$) cycles, the capacitance of the device remains no obvious changes, indicating the as-assembled supercapacitor not only possesses good flexibility, but also exhibits remarkable temperature tolerance.

Vanadium-based metal-organic framework (V-MOF) nanowire-bundle arrays was also reported as binder-free cathodes for high-rate and high-energy-density wearable Zn-ion batteries.^[103] He et al. prepared 3D conductive V-MOF on carbon nanotube fibers (CNTFs) through a simple one-step hydrothermal method as depicted in Figure 4b. With increase of the hydrothermal reaction time, the V-MOFs with a compact structure served as a self-sacrificed template, and gradually transformed into nanowire along the specific crystal faces via Ostwald ripening and self-assembling process, forming hierarchical nanowire bundle structures. Due to the large specific surface area and good conductivity of the active material V-MOF, the good mechanical flexibility and stitchability of CNTFs, the as-obtained V-MOF-48@CNTF//Zn battery exhibited good electrochemical stability and satisfactory flexibility for next-generation wearable electronics (Figure 4j).

In addition, 1D self-standing Ni-MOF-74 grown on carbon nanotube fibers (Ni-MOF-74@CNTF) as a binder-free cathode of Ni-Zn batteries was constructed by Man et al.^[104] As shown in Figure 4c1, Ni-MOF-74 possesses an open channel structure with pore diameter of $\approx 11 \text{ \AA}$. This unique 1D structure is very beneficial to enhance the permeability of electrolyte and reduce the steric hindrance, thus facilitates rapid electrolyte diffusion in the electrochemical reaction process. Figure 4c2 illustrates

the transportation process of ions and electrons. The SEM image in Figure 4f demonstrates that Ni-MOF-74 nanoarrays were highly aligned and well distributed on the CNTF surface with a cone-like structure. All these features endow Ni-MOF-74@CNTF with excellent electrochemical ability and flexibility, and consequently outstanding performance as a cathode of Ni-Zn battery (Figure 4k).

MOFs with multiple metal ion components, which could generate local defects and thus lead to electronic delocalization in the MOFs,^[105–108] were also explored as flexible electrode applications. For example, Zhou et al. demonstrated the preparation of self-supported multicomponent CPO-27 MOF nanoarrays, which was used as anode for lithium storage and exhibited high performance.^[109] The facile preparation process is illustrated in Figure 4e. The CPO-27 nanorods were uniformly aligned on the Ni foam substrate, which were thermally stable even after heating treatment (Figure 4g). With such a structure, the interaction between multiple metal components promotes electronic delocalization in CPO-27, thus increases the electronic conductivity.^[106,107] Moreover, coating a conductive layer on non-conductive substrate is a common strategy to overcome the conductivity barrier of pristine MOFs. Recently, Xu et al. also prepared ZIF-L coated PANI interweaved film on carbon fiber paper as a flexible electrode for supercapacitor.^[110]

Based on above-mentioned examples, clearly the direct application of MOF-based nanoarrays in flexible energy storage has the following advantages: 1) the phases of those MOF-based nanoarrays usually are simple, which is helpful to fully figure out the relationship between the electrochemical performance and the structures as well as the morphologies of the materials; 2) the electrical conductivities of these kinds of MOF-based nanoarrays are pretty satisfying, which helps enhance the electrochemical energy storage performance; 3) free of high-temperature process is an attractive feature during the preparation of such materials, which not only simplifies the preparation process of electrode materials, but also reduces energy consumption in high-temperature process.

However, in general, not many MOF-based nanoarray were produced due to the following reasons: first of all, currently only a few MOFs are electrical conductive, which inevitably restricts their potential utilization as flexible electrodes in electrochemical energy storage; second, the organic ligands used for MOF preparation are usually expensive, which limits their large-scale production; finally, the structure stabilities of these MOF-based nanoarrays are moderate or even poor, thus inevitably affect their cycling stability in electrochemical energy storage performance. As a result, increased attention is paid to MOF-derived nanoarray structures for flexible energy storage applications.

4. MOF-Derived Nanoarrays

The majority of pristine MOFs possess high porosity, large surface area, versatile functionalities, diverse structures, and controllable chemical compositions, which are beneficial to electrolyte penetration, ion transportation and incorporation of electroactive sites. However, their applications in energy storage field are hindered due to their poor electrical conductivity, low tap density, and irreversible structure degradation during the charge/discharge processes.^[111] Hence, most pristine MOFs are not appropriate

materials for electrodes. To address this conductivity issue, many post-processing approaches have been exploited and a variety of MOF derivatives have been synthesized. Usually, the most direct approach is the one-step heat treatment of MOF materials under controlled conditions (temperature, duration, and gas atmosphere et al), which leads to the formation of MOF-derived carbons, metal/metal oxide (M/MO) doped carbonaceous materials M@C, MO@C composites, metal sulfide, metal selenide, metal nitride or N doped metal compounds etc.^[35] The preparation and applications of those MOF-derived nanoarray structures in flexible electrochemical energy storage are discussed and summarized in this part.

4.1. Metal Oxide Nanoarrays

Metal oxides are widely considered as energy storage materials due to their low cost, natural abundance, environmental benign, variable oxidation states, favorable electrochemical activity, good stability and large theoretical-specific capacitance in redox reactions.^[29,112–115] Moreover, the simple preparation process and readily controllable morphology of metal oxides also make it easy to construct metal oxide nanoarray structures.^[116–121] Since a large variety of metal ions and ligands are available for the preparation of MOFs, various metal oxides can be derived from the as-prepared different MOFs. Generally, different preparation methods of MOFs and their derivatives may result in different morphologies and consequently different electrochemical performance. In this section, MOF-derived metal oxide nanoarray structures prepared via several typical strategies and their utilizations in flexible electrochemical energy storage are summarized as follows.

4.1.1. Hard-Templated Metal Oxide Nanoarrays

Among different metal oxide nanoarrays, nanostructured ZnO is widely explored as hard-template to fabricate ZnO-based nanoarray structures.^[122–126] For example, in 2015, for the first time Zhang et al. reported MOF derived ZnO@ZnO quantum dots (QDs)/C core-shell nanorod arrays (NRAs) utilized in lithium ion batteries.^[122] First, ZnO nanoarray on CC was prepared, then the prepared ZnO nanoarrays/CC was functioned as both the precursor and the hard template to induce ZIF-8 growth on the surface of ZnO nanoarrays. Finally, the vertically aligned ZnO@ZIF-8 NRAs was transformed into ZnO@ZnO QDs/C NRAs through one step heat treatment in N₂ atmosphere. In this process, the ZIF-8 derived ZnO QDs provide extra capacity, and the ZIF-8 derived carbon layer of a few nanometer can not only greatly enhance the electrical conductivity of the ZnO NRAs, but also efficiently endure the volume expansion and alleviate the pulverization problem of ZnO during the consecutive charging and discharging process. When used as anode in lithium ion batteries, the fabricated ZnO@ZnO QDs/C NRAs showed a high capacity of 785 mA h g⁻¹ at second cycle and maintained 500 mA g⁻¹ after 100 cycles, and it kept 89% of the first discharge capacity, implying excellent energy storage capacity and ultra-stable performance. Similarly, Li and coworkers used ZIF-8 derived ZnO@C arrays as skeleton to deposit

Zn and constructed CC-ZnO@C-Zn as binder-free anode for flexible Zn-Co batteries.^[124] The trilayer CC-ZnO@C-Zn anode with hierarchical 3D structures can well suppress Zn dendrite growth and maintain an ultra-stable cycling performance (71.1% after 5000 cycles). Very recently, Liu et al. also utilized ZIF-8 derived ZnO@C arrays as skeleton to load NiCo-LDH nanosheets, which was further selenized to form ZnO/C@(Ni,Co)Se₂ as cathode for flexible supercapacitor.^[125] The ZnO/C@(Ni,Co)Se₂ core-shell arrayed nanostructures presented excellent specific capacity of 164.18 mAh g⁻¹ at 1 A g⁻¹. In addition, the assembled ZnO/C@(Ni,Co)Se₂//AC asymmetric supercapacitor exhibited superior energy density of 65.67 W h kg⁻¹ at 800 W kg⁻¹.

In 2017, Yang et al. used ZnO nanorod arrays (ZnO NRAs) on nickel foam as both the hard template and the self-sacrificial precursor to load ZIF-8.^[127] ZnO NRAs not only provide Zn ions for the nucleation of ZIF-8, but also function as skeleton for the epitaxial growth of ZIF-8. The obtained ZnO@ZIF8 was further used as template for the preparation of ZnO@C@LDH and Fe₂O₃@C core shell NRAs respectively. The detailed preparation process of the ZnO@C@LDH and Fe₂O₃@C core shell NRAs is shown in Figure 5a. After high temperature pyrolysis of the prepared ZnO@ZIF8, the ZIF-8 layer was converted into porous carbon, leading to the formation of ZnO@C, which was then used as substrate for electrodeposition of CoNi-LDH nanoplatelet to obtain the cathode of ZnO@C@LDH with hierarchical structures. The introduced carbon layer of ZnO@C not only enhance the electrical conductivity of the composites, but also provide extra capacitance. Moreover, the carbon layer can also function as an ideal protecting layer since it firmly combines with the pseudocapacitance material, prevents the collapse of the metal oxide structure during long term charging and discharging cycles, thus results in good electrochemical stability of the composite. SEM image in Figure 5b shows that ZnO NRAs with diameter of ≈60 nm uniformly covered on the nickel foam substrate, and Figure 5c shows the ZnO@C@LDH core-shell NRAs with hierarchical structures. The electrochemical performance was evaluated and the GCD curves in Figure 5d showed that the ZnO@C@LDH exhibited enhanced capacitance, reached 6.2578 F cm⁻², almost 3.5 times that of ZnO@LDH electrode, manifesting the important role of the ZIF-8 derived carbon layer which greatly contributed to the electrochemical capacitance. In the case of the preparation of Fe₂O₃@C core shell NRAs, ZnO@ZIF8 was turned into Fe(OH)₃@ZIF-Fe via ion exchange, followed by pyrolysis. A flexible all-solid-state asymmetric supercapacitor based on the prepared ZnO@C@LDH as cathode and Fe₂O₃@C as anode was assembled. Such a supercapacitor not only showed superior cycle stability with 95.01% of capacitance retention after 10 000 cycles, but also exhibited good flexibility that it can light a red LED at bent state (Figure 5e).

Besides ZnO nanoarrays, other metal oxides such as TiO₂, CoO, Co₃O₄, NiCo₂O₄, FeCo₂O₄, CuO, ect. based nanoarray structures have also been prepared for flexible energy storage.^[118,128–135] Taking NiCo₂O₄ as an example, Li et al. reported NiCo₂O₄ nanowires on CC as template to load Ni-MOF as a cathode for flexible hybrid supercapacitor.^[130] Figure 5f shows the schematic illustration of the preparation of NiCo₂O₄@Ni-MOF core/shell hybrid arrays and the assembled NiCo₂O₄@Ni-MOF//active carbon (AC) hybrid supercapacitor (HSC) device. The GCD curves in Figure 5g suggest that the NiCo₂O₄@Ni-

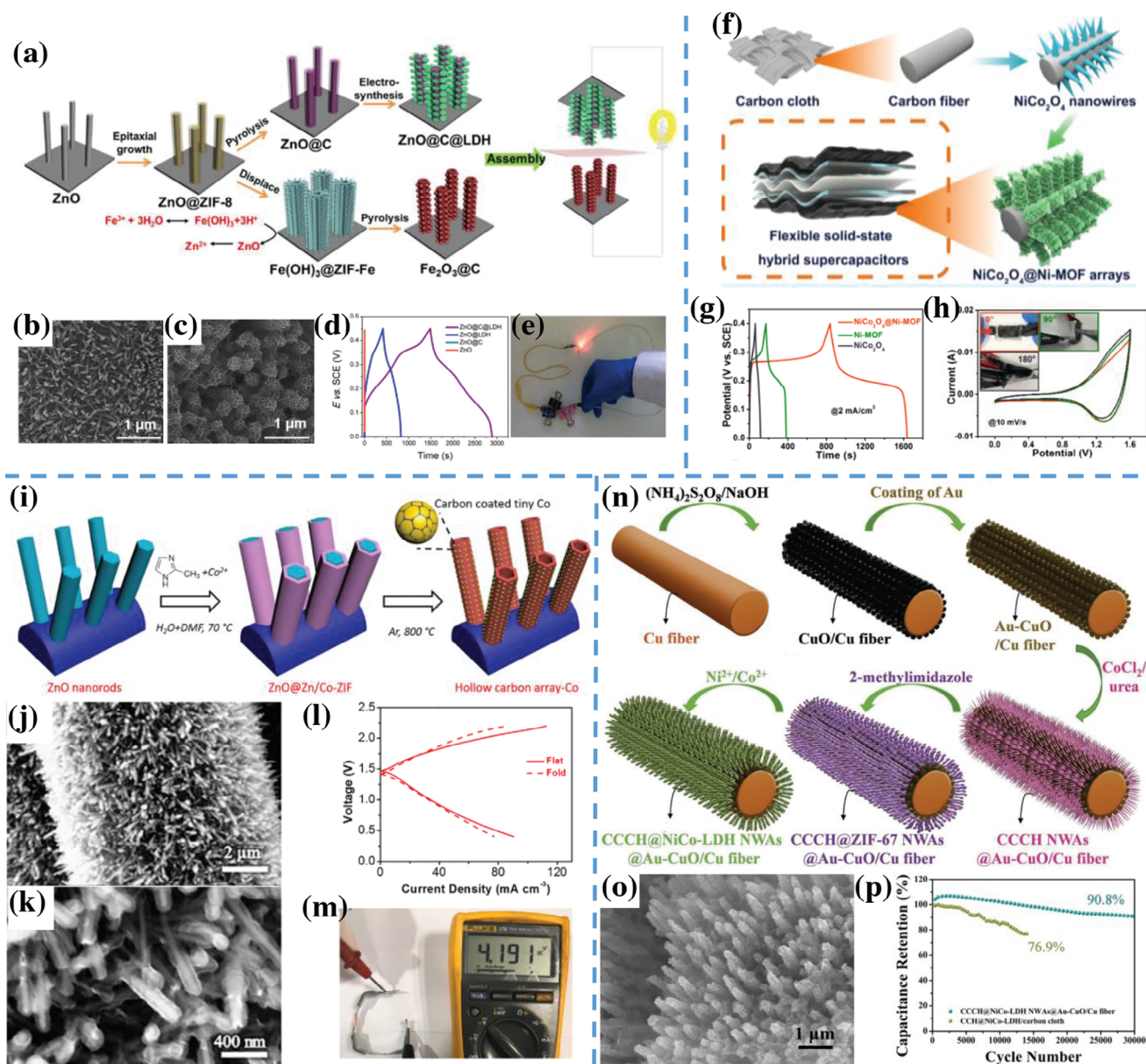


Figure 5. a) Schematic illustration of the fabrication of ZnO@C@CoNi-LDH and Fe₂O₃@C core-shell NRAs for asymmetrical FSSC. b) SEM image of ZnO NRAs. c) SEM image of ZnO@C@CoNi-LDH core-shell NRAs. d) GCD charge/discharge curves of the ZnO, ZnO@C, ZnO@LDH and ZnO@C@LDH NRAs. e) LED lighting demonstration, powered by two FSSC devices in series.^[127] Reproduced with permission. Copyright 2017, Elsevier. f) Schematic illustration of the synthetic approach for NiCo₂O₄@Ni-MOF core/shell hybrid arrays on carbon cloth. g) GCD curves of the carbon cloth, NiCo₂O₄, Ni-MOF (36 h) and NiCo₂O₄@Ni-MOF (12 h) electrodes at 2 mA cm⁻². h) CV curves recorded at 10 mV s⁻¹ under different bending conditions, inset showing the corresponding photographs of the device.^[130] Reproduced with permission. Copyright 2019, American Chemical Society. i) Schematic illustration of the fabrication process of HCA-Co nanoarrays. j,k) SEM images of ZnO@Zn/Co-ZIF-2. l) Discharge and charge polarization curves of HCA-Co-1 based solid-state Zn-air batteries under flat and fold status. m) Digital images showing three cells under fold status can generate a voltage of ≈4.19 V.^[136] Reproduced with permission. Copyright 2019, Elsevier. n) Schematic illustration of the synthesis of CCCH@NiCo-LDH NWAs@Au-CuO/Cu fibers. o) SEM images of CCCH@NiCo-LDH NWAs. p) Long-term cycling performance of the CCCH@NiCo-LDH NWAs@Au-CuO/Cu fiber and CCH@NiCo-LDH NWAs/CC.^[129] Reproduced with permission. Copyright 2019, Wiley-VCH.

MOF nanoarray electrode exhibited the longest discharge time among the three studied samples, indicating superior capacitance of the hierarchical NiCo₂O₄@Ni-MOF electrode. When matched with AC anode, the NiCo₂O₄@Ni-MOF//AC HSC device displayed good electrochemical stability and promising mechanical flexibility (Figure 5h).

The above discussed core-shell metal oxide array structures with coated MOF are basically solid structures, which inevitably hamper the transportation of electrolyte ions and hinder the electrochemical reaction reaching the inner part of the electrode. To tackle this issue, Zhu et al. attempted to synthesize MOF derived hollow carbon nanotubes (HCA) through using the porous

characteristics of MOF and the volatile characteristic of Zn at high temperature (boiling point 907 °C) which is formed via the reduction of ZnO by the in-situ produced carbons.^[136] The schematic preparation process of HCA-Co nanoarrays is illustrated in Figure 5i. The ZnO nanorod arrays act as template to grow bimetallic Zn/Co-ZIF shells. The SEM images in Figure 5i,j show that ZnO@Zn/Co-ZIF-2 nanoarrays with core-shell structure uniformly covered on the CC. After high temperature pyrolysis in inert atmosphere, ZnO was reduced by the in-situ formed carbon to volatile metallic Zn which vaporized at higher temperature, and hollow N-doped carbon nanotube arrays with confined Co nanoparticles were obtained. The HCA-Co nanoarrays were directly used as cathode for flexible Zn-air batteries, which performed very well under either flat or folded state (Figure 5l). The assembled three solid-state Zn-air batteries in series under bent status generated a voltage of ≈ 4.19 V (Figure 5m).

In addition, copper fiber with excellent electrical conductivity was also reported to be used as substrate to fabricate energy storage device. Guo et al. prepared multicomponent hierarchical Cu-doped NiCo-LDH/CuO double arrays on Cu fiber as cathode for flexible supercapacitor which exhibited ultralong cycling life.^[129] The schematic diagram of the preparation process of Cu-doped CCCH@NiCo LDH NWAs@Au-CuO/Cu is illustrated in Figure 5n. Through etchant treatment of an alkaline oxidative solution, the Cu fiber was etched and oxidized into CuO nanosheets, followed by coating an Au layer to improve the electrical conductivity. Afterwards, CoCu-LDH nanowires were anchored on the surface of Au-CuO nanosheets/Cu fibers and used as scaffold to grow ZIF-67 layer. Finally, Cu-doped CCCH@NiCo LDH NWAs@Au-CuO/Cu was obtained by ion exchange, and its SEM image is shown in Figure 5o. The as-prepared electrode exhibited ultra-long charge/discharge cycling stability and retained 90.8% of its capacitance after 30 000 cycles at 33.3 A g⁻¹.

4.1.2. Self-Templated Metal Oxide Arrays

Most MOFs are of good thermal stability, but after heat treatment of MOFs at high temperatures in controlled gas atmosphere, MOF derivatives with minor morphology change can be obtained. Direct pyrolysis of selected MOFs to obtain metal oxide arrays has been widely reported.^[112,137–140] For example, Zheng et al. reported a facile and scalable route for the in situ fabrication of ultrafine MnO nanocrystals embedded in porous carbon matrix (MnO@C), which was used as anodes for lithium-ion batteries, exhibiting a high reversible specific capacity of 1221 mAh g⁻¹ after 100 cycles at a current density of 100 mA g⁻¹.^[114] Tan et al. also prepared a Mn-MOF derived Mn₃O₄ with bulk oxygen defects (O_d-Mn₃O₄@C) through valence engineering, which was used as a cathode material for aqueous Zn ion battery with ultra-long cycle life.^[141]

In general, local electronic structure modified by oxygen defects only appear at the surface of the material, not in the bulk phase. However, Tan et al. successfully obtained Mn₃O₄ with bulk oxygen defects simply by calcining Mn-MOF nanoarrays in air. As shown in Figure 6a, O_d-Mn₃O₄@C nanoparticles gradually formed along with the decomposition of Mn-MOF under thermal treatment. The O_d-Mn₃O₄@C nanoparticles maintain the nanorod arrays of Mn-MOF (Figure 6b). Vaporization and car-

bonization of carbon species from lattice oxygen of crystalline MOF leaves behind oxygen defects during calcination of Mn-MOF, therefore, in situ carbon reduction produces not only oxygen defects on the surface of the material, but also abundant oxygen defects in the bulk phase. The presence of bulk oxygen defects can lead to the formation of octahedron oxide (MnO₆), which can inhibit the dissolution of Mn²⁺. Moreover, oxygen defects can also increase intrinsic conductivity of the material and provide more active sites for Zn²⁺ and H⁺ insertion. Hence, the Zn-ion battery assembled with O_d-Mn₃O₄@C NA/CC exhibits a high specific capacity (396.2 mAh g⁻¹) and an ultra-long cycle life (12 000 cycles) as shown in Figure 6c.

Very recently, Li et al. reported the preparation of Ni doped V₂O₅ nanowires (Ni-V₂O₅) by quenching V-MOF in cool salt solution.^[142] The as-prepared Ni-V₂O₅ with modified local electronic structure and V coordination environment, provided fast charge transfer and more Zn²⁺ storage/adsorption sites. Consequently, the aqueous fiber-shaped Zn-ion battery assembled with Ni-V₂O₅ as cathode exhibited superior rate performance and high energy density. When the flexible battery was integrated into a magnetically fibrous soft robot, it demonstrated promising potential to provide both energy storage and load-bearing capacity.

In addition, porous transition metal oxides (i.e., ZnO, Co₃O₄) nanosheet arrays derived from MOF coated 3D substrates (i.e., 3D nickel foam, carbon fiber) can be successfully synthesized by a facile liquid-phase deposition method followed by calcination.^[137,143] Guan et al. reported a kind of hollow Co₃O₄ nanosphere embedded in nitrogen doped carbon arrays on flexible carbon cloth (NC-Co₃O₄/CC), which was used as electrode for a solid-state Zinc-air battery.^[144] The preparation of NC-Co₃O₄/CC is shown in Figure 6d. NC-Co₃O₄/CC was obtained by two-step calcination of the Co-MOF on carbon cloth. SEM images of NC-Co₃O₄/CC in Figure 6e-f showed that the N-doped carbon nanowalls were decorated with numerous nanoparticles. An all-solid-state Zn-air battery was assembled using the NC-Co₃O₄ as a flexible air cathode, which delivered a high open circuit potential of 1.44 V, a capacity of 387.2 mAh g⁻¹, and excellent cycling stability with mechanical flexibility, and outperformed the Pt- and Ir-based devices (Figure 6h).

For energy storage devices, usually both cathode and anode are needed and the materials for both electrodes as well as their preparation methods vary largely, which makes the assembling of device complicated and difficult. In this regard, Guan and co-workers developed a “one for two” concept to simplify the procedure for the preparation of electrode materials, in which both cathode and anode of the supercapacitor are derived from 2D MOF nanoarrays.^[29] The detailed fabrication procedures and the architecture description are illustrated in Figure 6i. Lower temperature calcination of 2D Co-MOF leads to porous CC@Co₃O₄, and higher temperature pyrolysis results in nitrogen doped porous carbon. A quasi-solid-state supercapacitor, which was assembled using Co-MOF derived different porous materials as electrodes, exhibited high energy density, good flexibility, as well as long term cycling stability (as shown in Figure 6j,k).

Apart from single metal oxide arrays, some bimetallic oxide nanoarrays derived from MOFs were also developed.^[145–149] For example, Guan and co-workers synthesized hollow CC@NiCo₂O₄ flakes through ion-exchange/etching and subsequent calcination of vertically aligned Co-based MOF

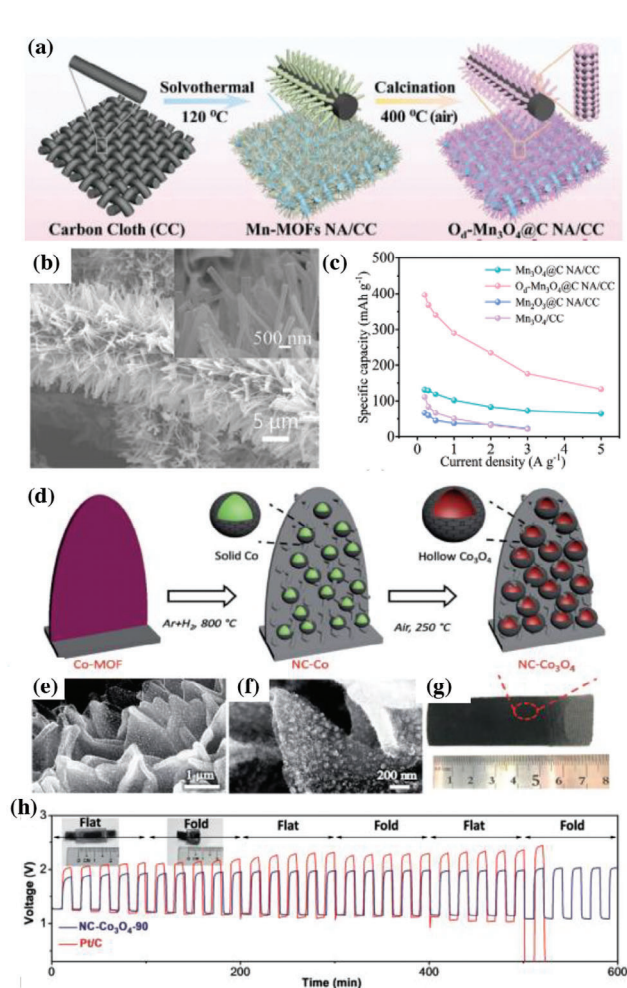
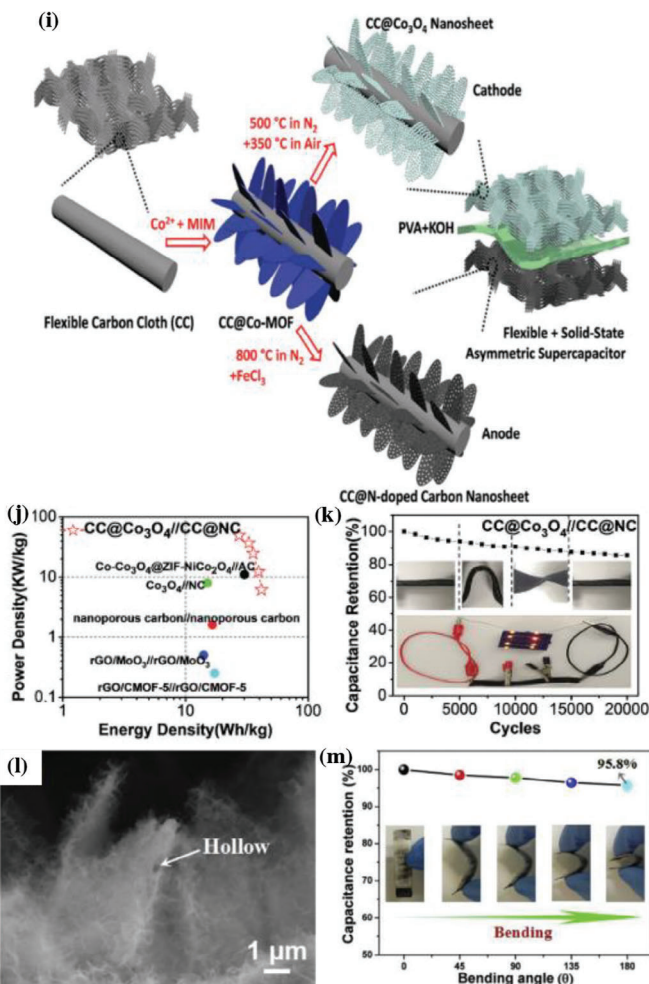


Figure 6. a) Schematic diagram of the synthesis procedure for O_d - Mn_3O_4 @C NA/CC nanostructure. b) SEM of O_d - Mn_3O_4 @C NA/CC. c) Specific capacity of batteries composed with various cathode materials at different current densities. Reproduced with permission.^[141] Copyright 2020, Wiley-VCH. d) Schematic illustration of the fabrication process for hierarchical NC- Co_3O_4 nanoarrays on carbon cloth. h) Mechanical flexibility and stability of the solid-state rechargeable Zn–air battery. Reproduced with permission.^[144] Copyright 2017, Wiley-VCH. i) Schematic illustration of the “one for two” fabrication process: 2D Co_3O_4 nanosheet cathode and N-doped carbon nanosheet anode obtained from the same Co-MOF precursor and assembled into a flexible asymmetric supercapacitor. j) Ragone plots, and k) cycling test result of the $CC@Co_3O_4//CC@NC$ asymmetric supercapacitor with PVA–KOH as gel electrolyte. Reproduced with permission.^[29] Copyright 2017, Royal Society of Chemistry. l) SEM image of Co-MOF derived $ZnCo_2O_4@NC$ NWAs. m) Capacitance retention for the asymmetrical supercapacitor device at different bending angles. Reproduced with permission.^[145] Copyright 2019, Elsevier.

nanoflakes.^[146] The supercapacitor using the as-obtained $CC@NiCo_2O_4$ with hollow and porous structure as electrode showed high capacitance and excellent rate capability. Moreover, the obtained $CC@NiCo_2O_4$ with hollow and porous structure exhibited superior OER electrocatalytic performance. Similarly, Kong et al. reported the preparation of ultrathin zinc-cobalt oxide nanoflakes anchored on N-doped carbon nanowall arrays ($ZnCo_2O_4@NC$ NWAs) from 2D Co-MOF nanowall arrays by controllable cation ion-exchange and post annealing strategies.^[145] The exchange of Zn^{2+} ions with Co^{2+} ions and the coordination of Zn^{2+} ions with organic linkers in Co-MOF result in the formation of Zn-Co precursor with core-shell structures. As shown in Figure 6l, after further carbonization and oxidation process, 3D self-branched $ZnCo_2O_4@NC$ with hollow nanowall arrays maintains the morphology of the precursor Co-MOF.



The obtained 3D $ZnCo_2O_4@NC/CTs$ could be directly used as a self-standing electrode for supercapacitor with good mechanical stability. When matched with $Fe_3O_4@r-GO/CTs$ anode, the assembled asymmetrical supercapacitor device showed very stable electrochemical performance at various angles (Figure 6m), demonstrating excellent flexibility and great potential in flexible energy storage area.

In contrast to high temperature calcination for the preparation of metal oxides from MOF precursors, many energy-saving methods such as electrochemical redox methods, ion exchange methods have been adopted.^[146,150–153] For instance, Chen et al. designed nickel–cobalt double hydroxide ($NiCo-DH$) supported on conductive nickel substrate.^[150] The prefabricated Co-MOF arrays supported on nickel foam served as cobalt ion source and the skeleton template. H^+ was released during the hydrolysis of

nickel ions, leading to further decomposition of Co-MOF and generation of NiCo-DH nanosheets on the microscale skeleton, which resulted in 3D hierarchical micro-nano sheet arrays on Ni substrate. The interlocked nanosheets not only ensure rapid electron transfer, but also facilitate fast electrolyte access and ion diffusion within the active materials. Due to the structural advantages, the optimized NiCo-DH electrode showed a high specific capacity of 303.6 mAh g^{-1} and outstanding rate performance (80% retention after 20-fold current increase). When the produced NiCo-DH nanosheets used as cathode in Ni-Zn battery, the device achieved a specific capacity of 329 mAh g^{-1} .

Tao and co-worker further demonstrated the transformation of MOFs into high-performance flexible metal oxide electrodes via a highly energy-saving and time-saving method.^[153] They subtly used an electrochemical oxidation method to fabricate amorphous hydroxyl-rich Co_3O_4 with hierarchical structure. When CV scan was applied within the potential range of oxygen evolution reaction (OER, $2\text{H}_2\text{O} \rightarrow \text{O}_2 + 4\text{H}^+ + 4\text{e}^-$), the Co-MOF, anchored on CC, was etched by H^+ generated from the OER process, which led to the decomposition of Co-MOF and the release of Co^{2+} and 2-HMINH⁺ into Na_2SO_4 electrolyte. It is ingenious that the released Co^{2+} was quickly oxidized by the oxygen generated from the OER process to form Co_3O_4 in situ. The Co_3O_4 -5 electrode prepared via this novel electrochemical oxidation method exhibited an outstanding rate capability and stable cycle performance. Zhang et al. also reported the synthesis of hierarchical and hollow $\text{Co}(\text{VO}_3)_2\text{Co}(\text{OH})_2$ composite leaf arrays on CC as supercapacitor electrodes through a one-step and energy-saving method.^[154] The as-prepared Co-V composites not only preserved the intrinsic leaflike shape of Co-MOF, but also had 3D hollow structures with irregular nanosheets on the outer surface. This unique hierarchical hollow and porous structures facilitated electrolyte penetration and promoted fast ion/mass transport with short diffusion distance, consequently enhanced the electrochemical performance significantly.

4.1.3. Sacrificial Templated Metal Oxide Nanoarrays

Direct assembly of active materials on CC is a promising way to fabricate flexible electrodes for energy storage. However, the overall surface area and mass loading of such electrodes are usually limited due to the hierarchical structures of the electrodes. In this regard, 2D metal-organic framework anchored on flexible substrate can meet the requirement of large specific area, flexibility and high mass loading after carbonization.^[155] Upon using MOF derived carbon arrays as substrate, the sites for growing active materials are greatly increased, and the equivalent series resistance is decreased. For example, Liu et al. utilized 2D MOF derived carbon nanoarrays grown on CC as a substrate to load active electrode materials, which achieved a flexible supercapacitor with high performance.^[155] Figure 7a,b show the schematic procedures and the actual appearance of the electrodes made in the study. After synthesis of Co-MOF on CC, one-step high temperature calcination and further etching of Co particles were carried out, leading to the transformation of 2D Co-MOF nanoflakes into N-doped carbon. Followed by electrodeposition or hydrothermal procedure, active materials MnO_2 and Bi_2O_3 were successfully decorated on the N-doped carbon flakes re-

spectively (Figure 7c,d). Thanks to the hierarchical structures, the flexible CC/MOFC/ MnO_2 and CC/MOFC/ Bi_2O_3 electrodes exhibited areal capacitance enhanced by $\approx 50\%$ and 100% , respectively (Figure 7e,f). Cai et al. adopted similar strategy and achieved uniform Fe_2O_3 nanoneedles anchored on the Co-MOF derived N-doped carbon nanoflakes.^[156] When matched with NiO/NC@CC cathode, the assembled supercapacitor showed good flexibility and stable electrochemical performance.

Recently, Peng et al. reported an aqueous supercapacitor, in which carbon coated Fe_3O_4 nanorods anchored on the hierarchical nanowall structured carbon was used as anode.^[157] The schematic illustration of material preparation process is presented in Figure 7g. The carbon coated Fe_3O_4 nanorod arrays and MnO_2 nanowire arrays uniformly covered on the MOF derived carbon nanowalls (Figure 7h,i). The produced CC/CW/ Fe_3O_4 @C anode exhibited an expanded operating voltage from -1.3 to 0 V and significantly enhanced specific capacitance (463 F g^{-1} at 1 A g^{-1}) due to the ultrathin carbon protection layer and the unique hierarchical structures. When matched with CC/CW/ MnO_2 , the assembled asymmetric aqueous supercapacitor could operate in a wide and stable voltage window of 2.6 V , and exhibited an ultrahigh energy density of 91.1 Wh kg^{-1} (Figure 7j), extraordinary rate capability and excellent cycle performance. Moreover, the assembled quasi-solid-state asymmetrical supercapacitor device based on CC/CW/ Fe_3O_4 @C as anode and CC/CW/ MnO_2 as cathode exhibited excellent electrochemical stability and mechanical stability (Figure 7k). In addition, Li et al. designed MOF derived Co_3O_4 @ NiCo_2O_4 nanosheet arrays as electrode in Li- O_2 batteries.^[149] Due to the well-defined 3D array structures that greatly facilitated O_2 diffusion and full electrolyte impregnation, together with the synergistic effect of NiCo_2O_4 and Co_3O_4 , the fabricated Co_3O_4 @ NiCo_2O_4 /CC cathode exhibited a very high specific capacity of $10\,645 \text{ mAh g}^{-1}$.

4.2. Metal Sulfide Nanoarrays

Transition metal sulfides have garnered extensive attention as promising electrode materials in recent years due to their advantages such as variable redox states, two orders of magnitude higher conductivity than their metal oxides, controllable microstructure and size, as well as attractive electrochemical performance.^[158–160] For example, NiS and CoS possess theoretical capacities up to 294 mAh g^{-1} .^[161] Although several nanostructured metal sulfides (such as NiS, CuS, CoS_2 and CoS) were synthesized and evaluated in batteries and supercapacitors, those active materials are normally in form of powder and thus need to be mixed with polymer binders to fabricate electrodes, which inevitably introduces undesirable interfaces and jeopardizes the nanosize benefits.^[161] Since the electrochemical properties of electrode materials are determined by the nature of the materials as well as their kinetic features, which are affected by the transportation of electrons and ions into the active materials, constructing nanoarray electrodes with direct mechanical and electrical contact with current collector is one of the most effective approaches to enhance the transport kinetics. It facilitates easy diffusion of ions, decreases internal resistance and consequently achieve high-power performance.^[161] Currently, there are only a few reports dedicated to metal sulfides

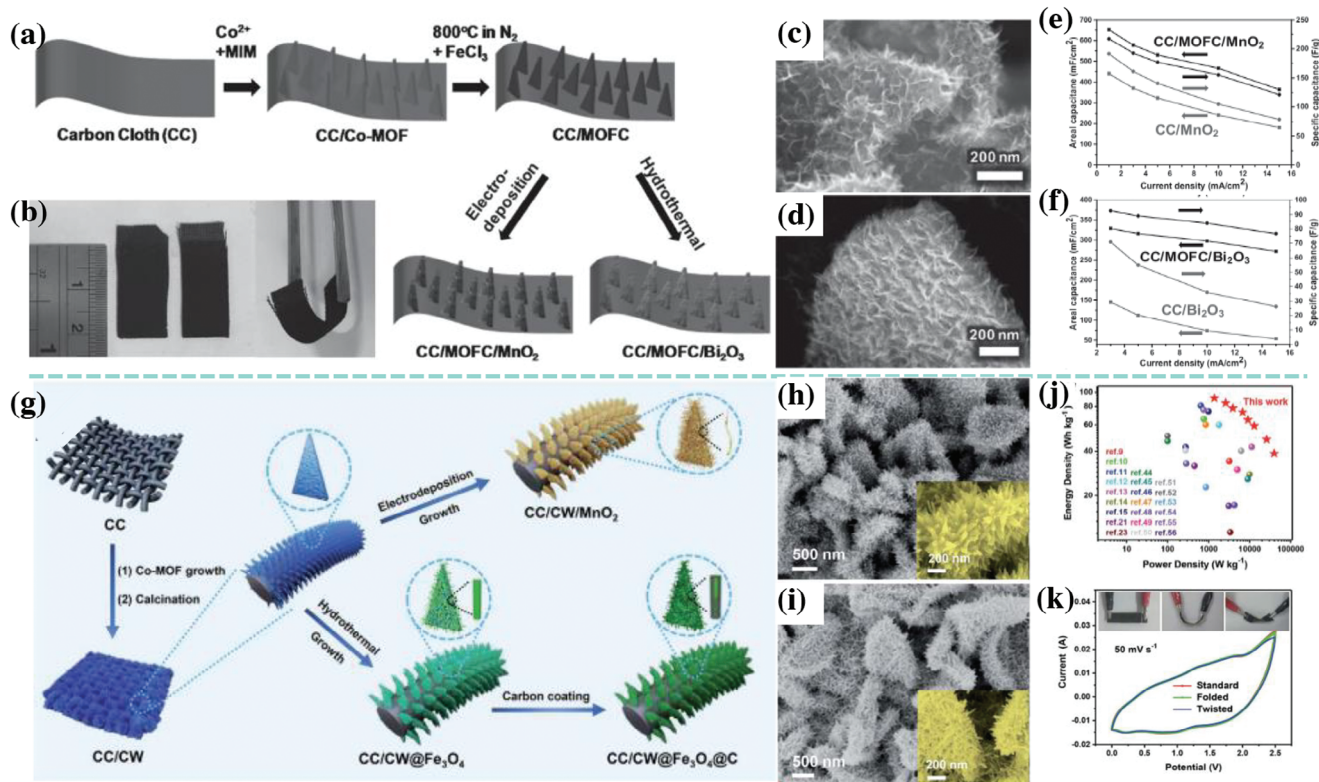


Figure 7. a) Schematic diagram of the fabrication process of MOFC-decorated electrode. b) Two digital images showing the size and flexibility of the electrodes. c) SEM image of CC/MOFC/MnO₂. d) SEM image of CC/MOFC/Bi₂O₃. e) Capacitance of MnO₂ with and without MOFC. f) Capacitance of Bi₂O₃ with and without MOFC. Reproduced with permission.^[155] Copyright 2018, Wiley-VCH. g) Schematic illustration of the fabrication process of hierarchical structured CC/CW/Fe₃O₄@C nanorod arrays and CC/CW/MnO₂ nanowire arrays. h) SEM image of CC/CW/Fe₃O₄@C NRAs. i) SEM image of CC/CW/MnO₂ NWAs. j) Ragone plot of the assembled asymmetrical supercapacitor compared with those previously reported samples. k) CV curves of the flexible asymmetrical supercapacitor under different bending status. Reproduced with permission.^[157] Copyright 2019, Royal Society of Chemistry.

nanoarrays directly attached to conductive substrates for high-rate battery/supercapacitor applications.

Thanks to the development of MOF nanoarrays with tailorable nature, high thermal stability and large porosity, some MOF-derived metal sulfide nanoarrays have been prepared and evaluated for applications in flexible energy storage.^[162–169] For example, Huang et al. used one step sulfurization of Zn-Co-ZIF on Ni foam to obtain Ni-Zn-Co-S nanosheet arrays for flexible supercapacitor.^[170] A similar strategy was adopted by Li et al. to synthesize P-doped ZCS/HC electrode. Due to the synergistic effect of N-doped C shells and P-doped metal sulfide, the resulting P-ZCS/HC possessed plentiful redox reaction sites, displays good conductivity and remarkable capacitance.^[171]

Making use of the solubility difference between the products, Yang et al. demonstrated to selectively prepare cobalt sulfide quantum dots (Co₉S₈-QDs) in Zn-MOF derived NiCoZn-LDH nanoarrays on carbon fiber (CF) for hybrid supercapacitor.^[172] **Figure 8a** presents the synthesis strategy of the CF@NiCoZn-LDH/Co₉S₈-QD nanosheet array electrode and the possible mechanism of selective vulcanization. The in situ prepared Co₉S₈-QDs offer more active sites, and the synergistic effect between Co₉S₈-QDs and NiCoZn-LDH provided improved electrochemical performance, such as capacitance retention, reversibility and cycling stability. As shown in **Figure 8b**, the hybrid supercapacitor based on the fabricated CF@NiCoZn-LDH/Co₉S₈-QD

cathode showed 95.3% capacitance retention after 8000 cycles. Similarly, CF@NiCo-alloy was also prepared from 2D Co-MOF flakes and sulfidized to generate NiCo-sulfide electrode.^[173] The interconnected NiCo-alloy@NiCo-sulfide core-shell structure endowed the electrode with highly exposed active sites and extraordinary electrochemical performance.

Moreover, a hierarchical CF@NiCoZn-S/NiCo₂S₄ composite originated from Zn-MOF nanoarrays on CF was designed and used as cathode for flexible supercapacitor.^[174] The 3D hierarchical nanoarray electrode with NiCoZn-S nanosheets coupled with granular NiCo₂S₄ nanowires uniformly covered on the carbon fiber exhibited excellent capacity of 194 mAh g⁻¹ at 1 A g⁻¹. Liu et al. directly vulcanized Co-MOF, which was then deposited on Co₃O₄ nanorods to produce Co₉S₈. The as-obtained Co₉S₈ nanoarrays showed ultra-long cycling stability, and maintained capacitance at 1.6 F cm⁻² after 100 K cycles.^[175] Wang et al. also prepared MOF-derived NiCo₂S₄ nanorods for supercapacitor.^[176] The NiCo₂S₄@CC exhibited capacitance of 879.6 F g⁻¹ at 1 A g⁻¹, which is higher than that of NiCo₂O₄@CC. Moreover, the NiCo₂S₄@CC electrode also presented excellent rate performance, and 88.7% capacitance retention was achieved when the current density was increased to 20 A g⁻¹. Interestingly, 2D MOF nanoflake derived N-doped carbon arrays were also explored as secondary substrate to load metal sulfides.^[177–180]

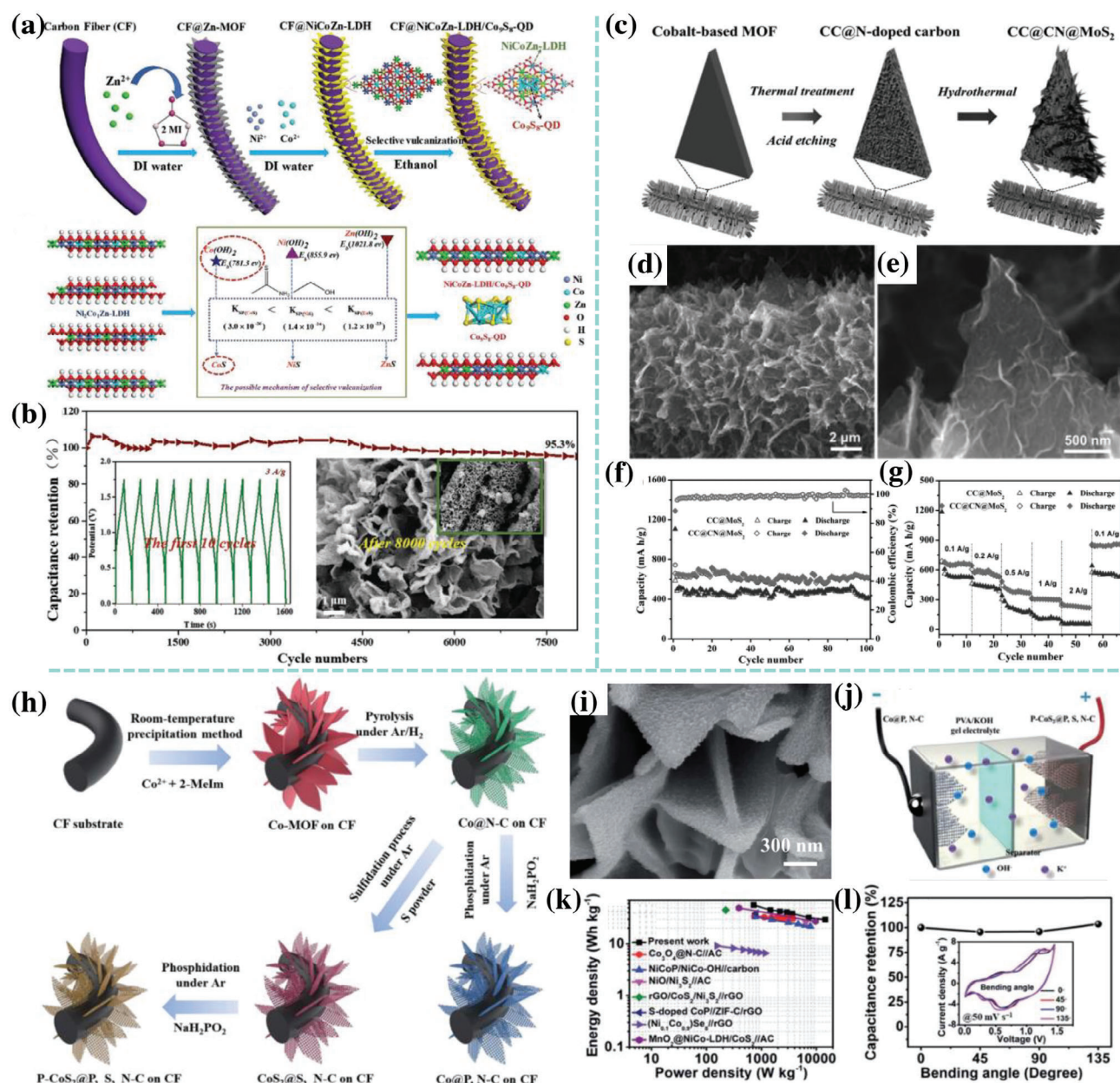


Figure 8. a) Schematic illustration of the fabrication of hybrid CF@NiCoZn-LDH/Co₉S₈-QD nanosheet arrays, the optimized atomic configurations and the possible mechanism of selective vulcanization. b) Cycling performance of the hybrid supercapacitor device at a current density of 3 A g^{-1} ; the inset shows the corresponding charge–discharge curves of the first ten cycles and the SEM images of the cathode material after 8000 cycles. Reproduced with permission.^[172] Copyright 2020, Wiley-VCH. c) Schematic illustration of the synthesis of the CC@CN@MoS₂ arrays. d, e) SEM images of CC@CN@MoS₂. f) Cycling performance of the CC@CN@MoS₂ and the CC@MoS₂ at 200 mA g^{-1} . g) Rate performance of the CC@CN@MoS₂ and CC@MoS₂ at various current densities. Reproduced with permission.^[181] Copyright 2017, Wiley-VCH. h) Schematic illustration of the fabrication of the P-CoS₂@P, S, N-C and Co@P, N-C nanosheets grown on the CF substrate. i) SEM image of P-CoS₂@P, S, N-C nanosheets. j) Schematic diagram of the as-fabricated P-CoS₂@P, S, N-C//Co@P, N-C asymmetrical supercapacitor device. k) Ragone plots of the fabricated asymmetrical supercapacitor device compared with the reported asymmetrical supercapacitor devices in the literature. l) Capacitance retention of the asymmetrical supercapacitor device at different bending angles. Reproduced with permission.^[179] Copyright 2019, Royal Society of Chemistry.

As a typical transition metal dichalcogenide with 2D layered structure, MoS₂ and related sulfides are promising materials for many electrochemical reactions and energy storage and conversion devices. Ultra-thin MoS₂ nanoflakes and carbon materials were successfully integrated by Ren et al. and used as high-

performance sodium ion battery anode.^[181] The schematic illustration of the synthesis process for CC@CN@MoS₂ is shown in Figure 8c. First, Co-MOF nanoflakes grew uniformly on CC with certain flexibility; then the nanoflakes transferred into N-doped nanocarbon chips with thickness of $\approx 110 \text{ nm}$ after thermal treat-

ment and ion etching. Finally, through hydrothermal reaction, ultrathin MoS₂ nanoflakes anchored on MOF derived N-doped carbon nanowalls (CN) were obtained (Figure 8d,e). The ultrathin nanoflakes can effectively shorten the ion transport path, thus the ions can be intercalated/delaminated more quickly. The heterostructure combined with carbon material can lead to quick electrolyte permeation and fast ion transfer, while porous carbon with N doping can avoid the aggregation of MoS₂. Moreover, the array structure can effectively hamper the volume expansion, ensuring the prepared electrode with high mechanical stability and good conductivity. Such a unique structure also alleviates the problems of rapid capacity attenuation, loss of active material and corrosion risk caused by the accumulation and aggregation of 2D MoS₂ layers, resulting in excellent performance in sodium ion storage. When tested as anode in a sodium ion battery, the CC@CN@MoS₂ arrays electrode not only exhibited 93.9% capacity retention at 613.7 mA h g⁻¹ after 100 cycles at 0.3 mA cm⁻², which is much higher than that of CC@MoS₂ (Figure 8f), but also showed a superior rate performance (Figure 8g).

Other transitional metal sulfide-based nanoarrays were also prepared from MOFs. Ren et al. reported TiO₂ encapsulated SnS₂ nanosheets on MOF-derived N-doped C (N-C) flakes for Na ion batteries.^[177] The synergistic effect of hybrid structure with open framework and the protective passivation layer of TiO₂ as well as the high capacity of SnS₂ nanosheets resulted in excellent rate performance and good cycling stability of the prepared TiO₂@SnS₂@N-C electrode. Liu et al. synthesized P-doped CoS₂ anchored on Co-MOF derived N-C skeleton. The illustration of preparation process is given in Figure 8h.^[179] SEM image in Figure 8i shows hierarchical structure with rough surface of P-CoS₂@P, S, N-C nanosheets, which would provide fast electrolyte ion transport. P doping could enhance the conductivity and reduce the adsorption energy of OH⁻ and Co species in P-CoS₂. The P dopant exhibited enhanced covalency, thus leading to the reduction of electron migration energy during the redox reaction. Moreover, the P-CoS₂ in nanoscale guaranteed rapid charge transfer. Consequently, the fabricated P-CoS₂@P, S, N-C electrode showed great rate capability and good cycling stability. The assembled flexible asymmetrical supercapacitor with P-CoS₂@P, S, N-C as cathode, and Co@P, N-C as anode (Figure 8j) delivered a considerable high energy density of 56.4 Wh kg⁻¹ at 725 W kg⁻¹ (Figure 8k). In addition, the device exhibited superior flexibility and there was negligible change of the shape of CV curves at different bent angles, as demonstrated in Figure 8l.

4.3. Metal Selenide Nanoarrays

Metal selenides, an important class of transitional metal chalcogenides, such as CoSe, CoSe₂, (Ni,Co)Se₂, NiV₂Se₄, NiFe₂Se₄ etc. exhibit excellent electrochemical energy storage capacity due to their superior electrical conductivity, promising electrochemical activity, lower band gaps and enriched redox sites compared to metal oxides, metal hydroxides or metal sulfides etc. As a result, they have been widely exploited as electrode materials for energy storage.^[125,182–188] However, the non-negligible volume expansion of metal selenide electrodes occurred during the long-term charge/discharge process usually causes severe pulverization and unstable solid-state interphase, thus leading to poor

cycling stability and inferior coulombic efficiency.^[189] To tackle these issues, incorporating metal selenides with carbonaceous materials has been considered as a promising strategy.^[190,191] In this respect, MOFs are ideal candidates as template or precursor to design and synthesize metal selenides/carbon hybrids as electrodes for energy storage.

For example, Zhang et al. fabricated a composite of hollow P-doped CoSe₂ nanoclusters embedded in MOF derived carbon flake arrays and applied it to Zn-air battery.^[192] The fabrication process is schematically illustrated in Figure 9a. Based on the TEM image in Figure 9b, the P-CoSe₂ hollow clusters with grain size of ≈20 nm were well confirmed. The obtained P-CoSe₂/N-C flake arrays exhibited excellent electrocatalytic performance for OER and ORR (Figure 9c,d). The synergism between the layered sheet arrays results in excellent dual functional electrocatalytic performance, showing a lower overpotential of 230 mV at 10 mA cm⁻² and a higher half wave potential (0.87 V). When the P-CoSe₂/N-C flake arrays were used as cathode to assemble an all-solid zinc-air battery, the device not only displayed high stable open circuit voltage but also possessed good mechanical flexibility.

Very recently, Xie et al. reported the preparation of bifunctional Co_{0.85}Se nanoparticles anchored on 2D Co-MOF derived nanoarrays as efficient sulfur host for Li-S batteries.^[193] Through a facile solution treatment and further selenization/carbonization, Co_{0.85}Se nanoparticles embedded in N-doped carbon nanoflakes were successfully covered on the carbon cloth (Figure 9e). SEM image in Figure 9f confirms interconnected N-doped carbon flake network, with many Co_{0.85}Se nanoparticles on the surface. The interconnected nanoflake network with numerous pores not only facilitated full contact between the Co_{0.85}Se active sites and the electrolyte, ensured rapid diffusion of lithium ions and fast transport of electrons, but also well accommodated the S₈ molecules and alleviated the volume change. Figure 9g shows the CV curves of CC-S, CC/NC-S and Co_{0.85}Se/NC-S. All samples exhibited similar redox peak positions, but Co_{0.85}Se/NC-S exhibited the highest reduction current intensity, indicating Co_{0.85}Se/NC-S is the most active materials under the same conditions. The rate performance in Figure 9h verified the good kinetic behavior of the prepared Co_{0.85}Se/NC-S. Similarly, Zhu et al. selenized Co-MOF derived Co-NC to prepare NC@CoSe₂ and used the produced material as cathode for aqueous supercapacitor. When combined with Co-NC@Fe₂O₃ anode, the supercapacitor device output a high power density of 23.5 KW kg⁻¹.^[191]

Tang et al. explored 2D MOF-derived Co_xO_ySe_z@C/CC for flexible alkaline Zn batteries applications.^[194] As depicted in Figure 9i,j, electrochemical analysis suggested that Co³⁺/Co⁴⁺ redox pair was the principal contributor to the capacity and voltage plateau in alkaline Zn batteries. Moreover, Se-doping not only enhanced the conductivity, but also sustained abundant and stable Co³⁺ species in the fabricated Co_xO_ySe_z@C/CC. Therefore, the alkaline Zn batteries with Co_xO_ySe_z@C/CC cathode exhibited high working voltage plateau, excellent areal capacity and immense ultra-long cycling lifespan compared to its low valence oxide counterpart. SEM image in Figure 9k shows the leaf-like CoSe_{2-x}@C sheets derived from ZIF-67 maintained the nanoarray structure and uniformly covered on the carbon cloth, which is beneficial to the permeation of electrolyte. The CV curve of Co_xO_ySe_z@C/CC in Figure 9l shows

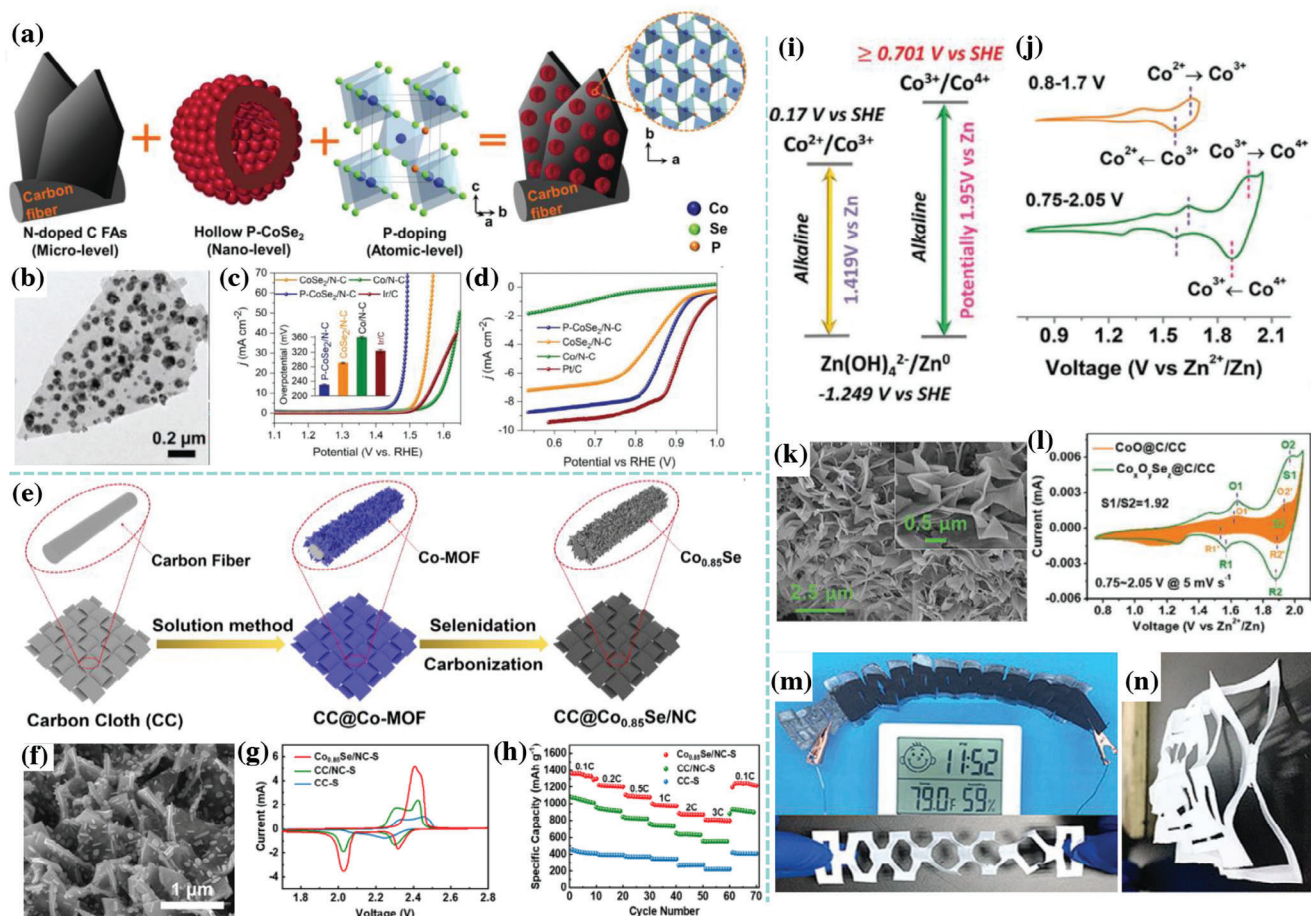


Figure 9. a) Schematic illustration of the hierarchical P-CoSe₂/N-C flake array structure. b) TEM image of P-CoSe₂/N-C. c,d) LSV curves of P-CoSe₂/N-C and other samples for OER and ORR, respectively. Reproduced with permission.^[192] Copyright 2018, Wiley-VCH. e) Schematic illustration of the fabrication process for Co_{0.85}Se/NC. f) SEM image of CC@Co_{0.85}Se/NC. g,h) CV profiles and rate performance of CC-S, CC/NC-S and Co_{0.85}Se/NC-S, respectively. Reproduced with permission.^[193] Copyright 2021, American Chemistry Society. i) Schematic illustration of a higher voltage plateau of Co³⁺/Co⁴⁺ redox pair compared with Co²⁺/Co³⁺ counterpart; j) schematic illustration of the triggered Co³⁺/Co⁴⁺ redox pair enabling a widened operating voltage. k) SEM image of CoSe_{2-x}@C/CC. l) CV curves of Co_xO_ySe_z@C/CC and CoO@C/CC. m,n) Optical photos of a thermometer-humidometer powered by different stretched models. Reproduced with permission.^[194] Copyright 2020, Wiley-VCH.

two pairs of redox peaks which were ascribed to Co³⁺/Co²⁺ and Co⁴⁺/Co³⁺, respectively. The peaks related to the Co⁴⁺/Co³⁺ pair (corresponding to the O2/R2 in Figure 9l) are significantly larger than those of Co³⁺/Co²⁺ pair (O1/R1 in Figure 9l), indicating the larger capacity contribution of the Co⁴⁺/Co³⁺ pair. In addition, the area of CV curve for Co_xO_ySe_z@C/CC is almost 2 times of that of CoO@C/CC, confirming the appreciable advantage of Co_xO_ySe_z@C/CC in terms of the areal capacity. When Co_xO_ySe_z@C/CC was used as cathode to assemble an aqueous quasi-solid state Zn battery, the as-assembled device showed extraordinary flexibility that it could power an electronic thermometer-humidometer in different stretched states (Figure 9m,n).

4.4. Metal Nitride Nanoarrays

Transitional metal compounds are commonly used as active materials to enhance energy density and overall performance of su-

percapacitors and batteries. However, compared to carbon-based materials, transition metal oxide/hydroxide compounds generally possess poor electrical conductivity and therefore exhibit suppressed energy storage performance. Metal nitride is an alternative class of materials, some of which have shown metal-like high electrical conductivity and can therefore accelerate charge transportation when used as an electrode material.^[147,195–197] Since the electronic energy state level of N 2p orbitals in nitride materials is higher than that of O 2p orbitals, N-doped metal oxides can have high electronic conductivity by lowering the band gap or overlapping the conduction and valence bands.

Metal nitrides have been recognized as a class of desirable electrode materials due to their high electrical conductivity and structural stability. When used as electrode during charge/discharge cycling, metal nitride nanoarrays derived from MOF provide sufficient accessible reaction sites as well as facile electron transportation pathway. Importantly, the metal nanoparticles embedded in nitrides can further enhance the conductivity for electron transport, and therefore improve electrochemical perfor-

mance. For example, Guan et al. prepared 2D NC-Co/CoN_x nanoarrays on carbon cloth through two pyrolysis steps and applied it as cathode in zinc-air batteries.^[198] After pyrolysis in Ar/H₂ atmosphere at high temperature, Co-MOF nanoarray flakes were converted into Co nanoparticles embedded N-doped carbon (NC) flakes without morphology change. Followed by nitridation in NH₃ atmosphere, the Co species were partially transformed into CoN_x compounds, resulting in an N-doped carbon nanosheet arrays decorated with Co/CoN_x nanoparticles. The well-integrated NC-Co/CoN_x electrode material with the merits of N-doped carbon, Co and CoN_x components, exhibited outstanding ORR and OER performance in alkaline media. Moreover, such NC-Co/CoN_x nanoarrays could grow on carbon microfibers to assemble fiber-shaped solid-state zinc-air batteries and showed enhanced volumetric power density and good flexibility.

Ni-doped Co-Co₂N@CC was produced via annealing of MOF-derived NiCo₂O₄ in NH₃ atmosphere by Liu et al., during which the 2D nanoarrays in MOF derivative maintained intact, and metal-metal nitride heterostructures were successfully established, as presented in **Figure 10a,b**.^[147] The GCD curves in **Figure 10c** showed that Ni/Co-N-350 has the longest discharge time among all the samples, indicating it possessed the highest specific capacity. Benefiting from the nanoflake frameworks and the metal-metal nitride heterostructures, the as-prepared Ni-doped Co-Co₂N exhibited a high specific capacity of 361.93 C g⁻¹.

Besides transition metal nitrides that can generally be produced via nitridation of MOF-derived composites directly, more complicated metal nitride composites have been fabricated by using MOF-derived carbon skeleton as second substrate. Huang et al. reported the preparation of hierarchical carbon-coated porous vanadium nitride nanosheet arrays on MOF-derived carbon wall (CC/CW/p-VN@C) composites and its application as an anode in aqueous asymmetric supercapacitors.^[199] First, V₂O₅ was prepared on Zn/Co-MOF@CC derived carbon walls (CW) through hydrothermal method, then the CC/CW/p-V₂O₅ was converted into CC/CW/p-VN after nitridation in NH₃ atmosphere. Finally, a thin carbon layer was coated to enhance the cycling stability of CC/CW/p-VN. The anode made with the resulting CC/CW/p-VN@C arrays exhibited a wide working window and remarkable long-term cycling performance. As shown in **Figure 10e**, CC/CW/p-VN@C could work steadily in the working window of -1.3–0 V, with specific capacitance as high as 605 F g⁻¹ achieved at a current density of 1 A g⁻¹, which was higher than those in the working window below -1.2–0 V, and much higher than that of CC/p-VN under the same conditions (239 F g⁻¹). Impressively, even at a higher current density of 60 A g⁻¹, the CC/CW/p-VN@C anode exhibited eminent rate performance under -1.3 to 0 V. To match with CC/CW/p-VN@C anode, CC/CW/Na_{0.5}MnO₂ cathode was prepared by electrodeposition of Mn₃O₄ on carbon walls, followed by electrochemical oxidation of Mn₃O₄ to Na_{0.5}MnO₂. The as-prepared CC/CW/Na_{0.5}MnO₂ could also work steadily in the range 0–1.3 V. Hence, an aqueous asymmetrical supercapacitor based on the above anode and cathode (as illustrated in **Figure 10d**) achieved working voltage up to 2.6 V. The hierarchical nanosheet/wall structures facilitate the electrodes with large specific surface and high mass loading as well as short ion and electron diffusion path, thus realize re-

markable electrochemical performance in the assembled asymmetrical supercapacitor.

Ligand exchange is widely adopted to adjust the electron structure of MOFs materials. Xu et al. synthesized Co/Fe-MOF nanoarray flakes by immersing 2D Co-MOF into K₃[Fe(CN)₆] aqueous solution.^[200] In this process, the 2D Co/Fe-MOF was formed by ligand exchange reaction between [Fe(CN)₆]³⁻ and 2-methylimidazole.^[201] After a facile combined carbonization-ammonization process, Fe, N co-doped FeCo₄N@N-C nanosheet array on CC was successfully constructed (**Figure 10g,h**). The introduced [Fe(CN)₆]³⁻ ligand could not only generate ideal pyridinic-N-M active sites, but also motivated the in-situ formation of N-doped carbon with defects during carbonization. The strong coordination effect between the Fe-Co₄N and N-C provided a large number of pyridinic-N-M species as active sites for ORR. The enriched Co³⁺ sites could also motivate the formation of targeted *OOH intermediates during OER with fast charge transfer (**Figure 10f**). Consequently, the produced Fe-CoN₄@N-C electrocatalyst exhibited superior catalytic activity toward OER and ORR in KOH media (**Figure 10i,j**). Meanwhile, a flexible Zn-air battery fabricated by using the self-supported Fe-CoN₄@N-C composite array as cathode showed a high volumetric power density of 72 mW cm⁻³ and good cycling durability.

In recent years, the application of metal-nitrogen carbon (M-N-C) single atom catalysts (SACs) with promising ORR and OER performance as cathode materials for metal-air batteries have attracted widespread interest, since SACs possess the merits of both heterogeneous and homogeneous catalysts, which enables the utilization of atom efficiency to be maximized. The formation of M-N_x sites not only optimize electronic structure of metal atoms but also enhance their stability.^[202–204] Making use of the high porosity and good thermal stability of MOF materials as well as high catalytic activity of Co SACs, Zang et al. developed single Co atoms anchored on N-doped porous carbon as cathode for Zn-air battery.^[205] As illustrated in **Figure 11a**, following a simple carbonization and a further acid treatment processes, Co-MOF nanoflakes grown on CC were transformed into Co single atoms anchored on nitrogen-doped porous carbon nanoflake arrays. The Co single-atom sites were coordinated with N to form stable Co-N_x sites anchored in the porous carbon flakes, and extra porosity together with active surface area were created by the removal of Co metal clusters (**Figure 11b**). Thus, the obtained NC-Co SAC nanoflake arrays exhibited a lower OER overpotential and much higher ORR saturation current than that of NC-Co containing excess amount of Co nanoparticles. Due to the bifunctional electrocatalytic activity of NC-Co SAC, the as-assembled solid-state Zn-air battery presented long cycling stabilities, high open circuit potential, good mechanical flexibility and high power density (**Figure 11c,d**).

Isolated iron sites coordinated with nitrogen-doped carbon (Fe-N-C) SACs deposited on CC substrate as self-supporting electrode for flexible aluminum-air battery was another example.^[206] Making use of the sublimation of ferrocene at low temperature and N-C skeleton produced from pyrolysis of Zn-MOF at high temperature, iron single atoms anchored on N-C (Fe-SA-NC) flakes was achieved through programmed temperature controlled treatment of ferrocene and Zn-MOF@CC (**Figure 11e**). The resulting Fe-SA-NC@CC displayed remarkable ORR activity and high durability (**Figure 11f**). When Fe-SA-NC@CC was used

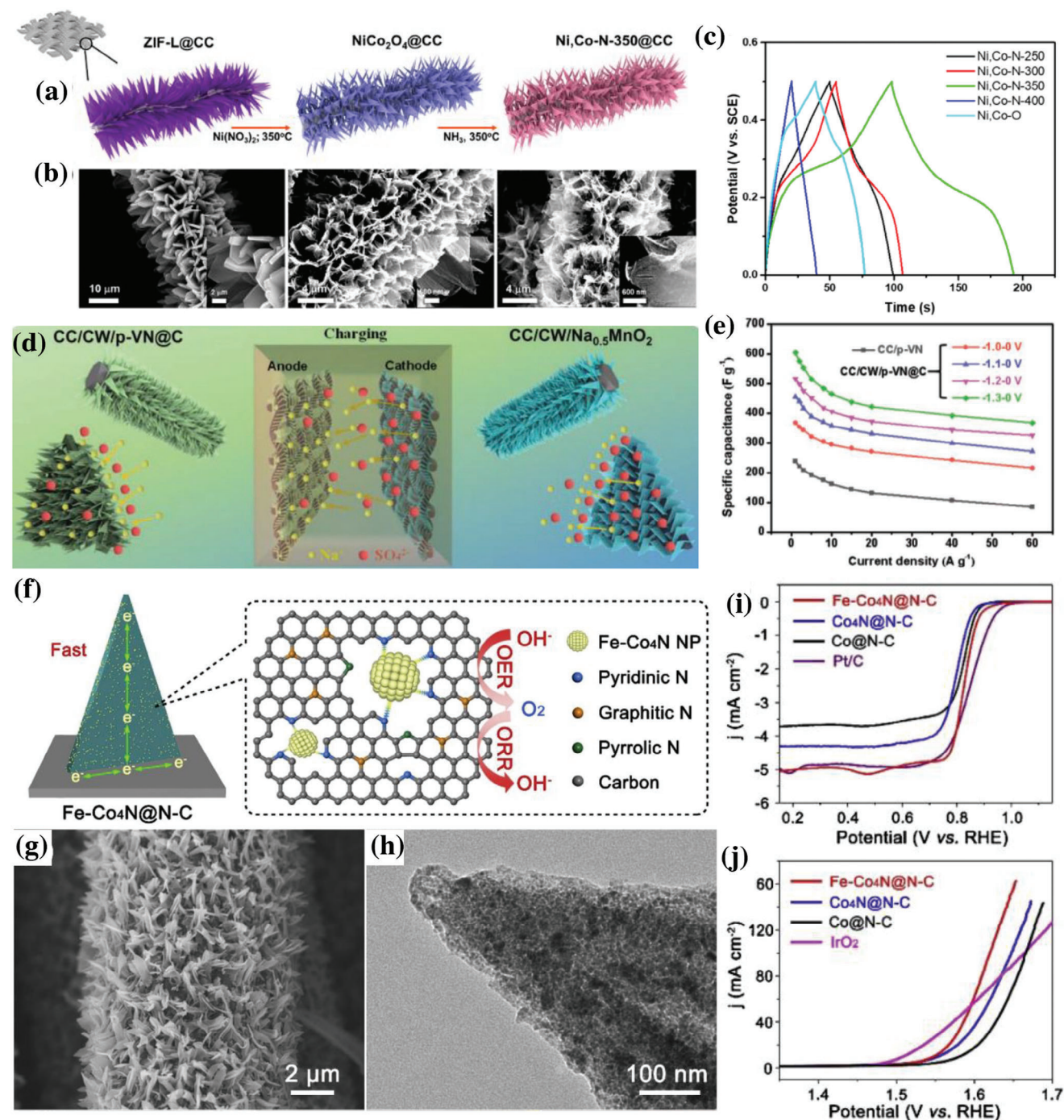
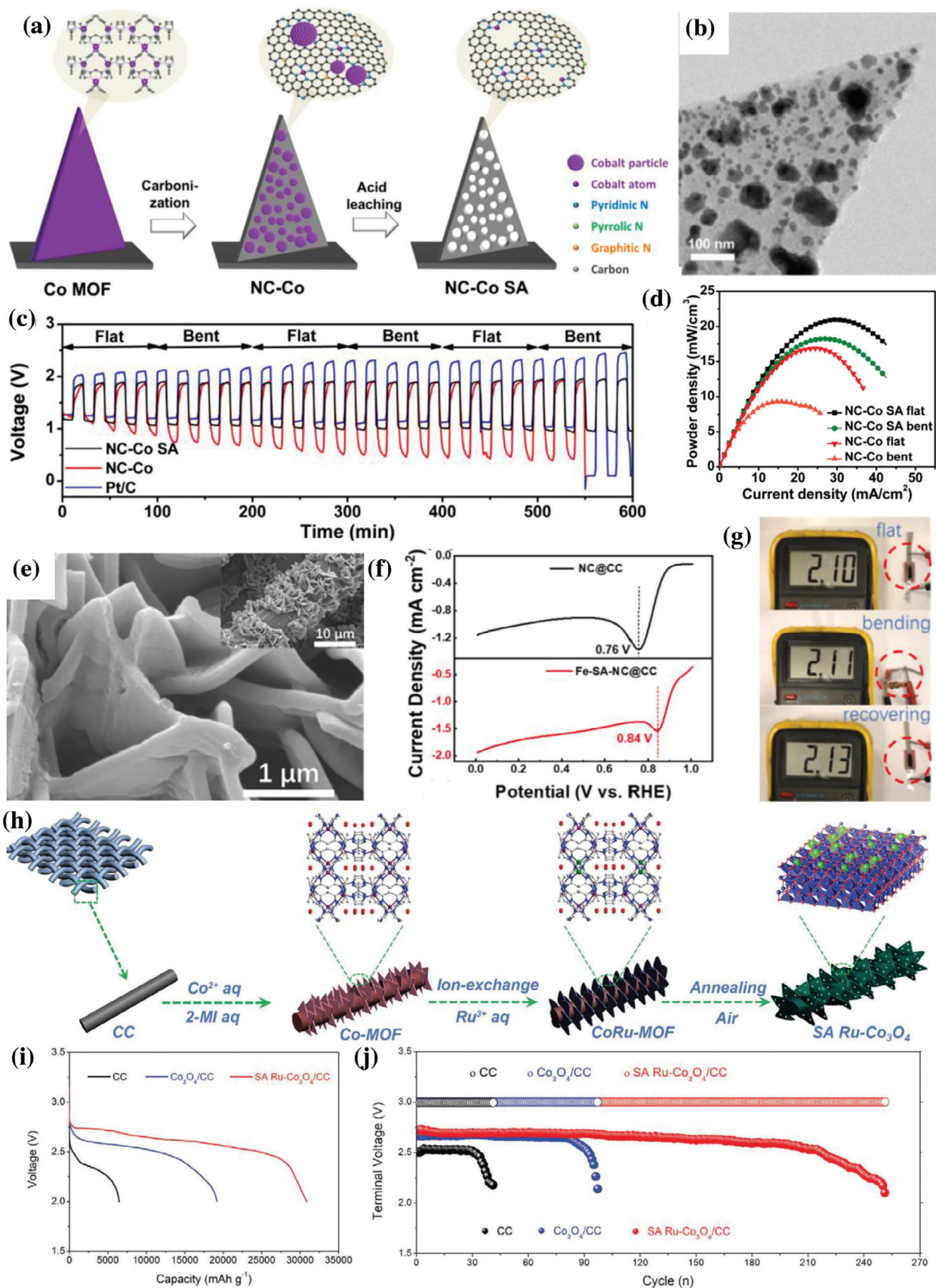


Figure 10. a) Schematic illustration of experiment procedure. b) SEM images of ZIF-L@CC, NiCo₂O₄@CC and Ni/Co-N-350@CC. c) GCD of nitride samples and their oxide counterpart. Reproduced with permission.^[147] Copyright 2018, American Chemical Society. d) The electrode design and charging process of the CC/CW/p-VN@C anode and the CC/CW/Na_{0.5}MnO₂ cathode in the assembled aqueous asymmetrical supercapacitor system. e) The specific capacitances of CC/p-VN in -1.3 to 0 V, and CC/CW/p-VN@C electrodes in various potential windows of -1.0 to 0, -1.1 to 0, -1.2 to 0 and -1.3 to 0 V at various current densities. Reproduced with permission.^[199] Copyright 2019, Wiley-VCH. f) Schematic illustration of Fe-Co₄N@N-C nanosheet grown on carbon cloth for dual-functional oxygen reactions. g) SEM image and h) TEM image of Fe-Co₄N@N-C electrocatalyst. i) ORR polarization curves tested at 1600 rpm of Fe-Co₄N@N-C, Co₄N@N-C, Co@N-C and Pt/C electrocatalysts. j) OER polarization curves of Fe-Co₄N@N-C, Co₄N@N-C, Co@N-C and IrO₂ electrocatalysts. Reproduced with permission.^[200] Copyright 2019, Elsevier.



as cathode to assemble a flexible aluminum-air battery, an impressive open-circuit voltage of 2.1 V was achieved even in bending state (Figure 11g).

Apart from metal-air batteries, single-atom catalytic materials can also be applied to other kind of energy storage devices, such as Li-CO₂ battery. Li-CO₂ battery has attracted extensive attention because it possesses not only high theoretical energy density (1876 Wh kg⁻¹), but also the ability to fix and consume greenhouse gas CO₂. Lian et al. demonstrated Ru single-atom implanted on MOF-derived Co₃O₄ nanoarrays as an efficient dual-catalyst for Li-CO₂ batteries.^[207] The synthesis process of SA Ru-Co₃O₄/CC is illustrated in Figure 11h. After ion-exchange and further calcination process, the obtained SA Ru-Co₃O₄/CC preserved well nanoarray structures from its MOF precursor. The 3D structured SA Ru-Co₃O₄/CC with large surface area could provide enough space for electrolyte and gas transport, as well as the storage of discharge products. Li-CO₂ batteries based on SA Ru-Co₃O₄/CC, CC and Co₃O₄/CC electrodes were assembled to evaluate their performance in electrochemical energy storage. The discharge curves of those Li-CO₂ batteries assembled from different cathodes at current density of 100 mA g⁻¹ are shown in Figure 11i. Interestingly, the battery with SA Ru-Co₃O₄/CC cathode delivered the highest capacity of 30 915 mAh g⁻¹, which was much higher than that of CC and Co₃O₄/CC cathode batteries. Moreover, Li-CO₂ batteries with SA Ru-Co₃O₄/CC cathode maintained 251 cycles at current density of 200 mA g⁻¹, superior to that of CC (41 cycles) and Co₃O₄/CC (97 cycles) cathode batteries (Figure 11j). The significantly enhanced cycling stability of Li-CO₂ batteries with SA Ru-Co₃O₄/CC cathode was attributed to the atomically dispersed Ru atoms that optimized the discharge product growth pathway and enhanced the catalytic activity.

4.5. Metal Phosphide Nanoarrays

Metal phosphides have shown excellent performance and great potential in electrochemical applications, which has been demonstrated by plenty of reports published in recent years.^[208–210] In particular, various metal phosphides have been utilized in electrochemical energy storage and conversion field.^[210–213] For example, Ren et al. synthesized multi-metal based carbon nanorods with hierarchical porous structure for Zn-air batteries.^[214] In this report, Fe₂Ni-MIL-88 nanorods were first prepared, then covered with a layer of ZIFs, finally were turned into dual MOF-derived FeNiCo@NC-P via high temperature carbonization and further phosphorization process. Owing to the synergetic effect of hierarchical porous structures and multi-metal components, the prepared FeNiCo@NC-P showed superior catalytic activity for both ORR and OER, and a low voltage gap was observed when it was used as a cathode in Zn-air batteries.

Wang et al. reported the fabrication of a self-supported CC@CoP/C-S derived from a 2D Co-MOF precursor and the use

of it as flexible cathode in Li-S batteries. The schematic illustration of the synthesis procedure is displayed in Figure 12a.^[215] The SEM image of CC@CoP/C-S (Figure 12b) showed that CoP/C-S nanoarrays uniformly covered on CC. This artful structure not only ensured high electrical conductivity due to the conductive matrix of CC and carbon nanoarrays, but also achieved synergistic effect due to the confinement of both the physical adsorption and the chemical interaction of polysulfides. Meanwhile, CoP nanocrystals embedded in carbon nanoarrays catalyzed the reduction of lithium polysulfides. Furthermore, these hollow carbon nanosheet arrays with large void space not only enhanced the amount of mass loading of sulfur, but also effectively buffered its volume expansion during the lithiation process. Due to such a unique structure, the fabricated CC@CoP/C-S cathode showed excellent cycling stability and high specific capacity at different current rates (Figure 12c,d) in Li-S batteries. In addition, Li-S pouch cells fabricated with the as-prepared CC@CoP/C-S cathode could be curved in different angles, showing remarkable flexibility (Figure 12e,f). A similar procedure was adopted by Xiao et al. to prepare Co-MOF-derived N-doped carbon nanosheet arrays embedded with CoP nanoparticles, which was used as cathode for Li-S batteries.^[213] Co-MOF derived CoP anchored on highly conductive and high N content of PAN-CNT fibers was also produced and used as highly efficient trifunctional electrocatalyst and cathode for Zn-air batteries.^[211]

Though MOF derived metal compounds have been widely exploited in energy storage, all-MOF derived battery materials anchored on substrate were seldom reported. Zhang et al. demonstrated the preparation and application of all-MOF derived battery materials on CNT fibers (CNTF) in wearable energy storage device.^[216] As presented in Figure 12g, CNTF with good conductivity and remarkable mechanical flexibility was used as substrate and collector, then ZnCo-MOF and Fe-MOF were covered on the collector, respectively. After different post-processing treatments, both ZnCo-MOF-derived NiZnCoP@CNTF cathode and Fe-MOF-derived S-α-Fe₂O₃/OCNTF anode were obtained. Typically, the NiZnCoP@CNTF cathode showed nanoarray flake structures with rough surface (Figure 12h), which was beneficial to larger surface area with more exposed active sites. The rate performance of NiZnCoP@CNTF and NiCoP@CNTF electrodes (Figure 12i) indicated that NiZnCoP@CNTF exhibited not only much higher specific capacity, but also better capacity retention ability. When the all-MOF-derived NiZnCoP@CNTF was used as cathode and S-α-Fe₂O₃/OCNTF as anode to assemble a wearable device, it could be well knitted in the textile and power a LED light (Figure 12j). In addition, the assembled device could also output electrochemical energy stably, without obvious capacity decay under various bending angles (Figure 12k), implying outstanding mechanical flexibility.

The high theoretical specific capacity values and prominent thermal stability of transition metal phosphides enable them as a class of promising candidates for energy storage, but there

Figure 11. a) Schematic illustration of fabrication process of NC-Co SA. b) STEM image of NC-Co SA. c) Mechanical flexibility and stability tests with continuous mechanical alternation of flat and bent states of NC-Co SA, NC-Co and Pt/C. d) Power–current density curves of NC-Co SA and NC-Co. Reproduced with permission.^[205] Copyright 2018, American Chemical Society. e) SEM image of Fe-SA-NC@CC. f) LSV curves of NC@CC and Fe-SA-NC@CC. g) Photographs of the open-circuit voltages of the aluminum-air battery working at flat, bending, and recovering states. Reproduced with permission.^[206] Copyright 2021, Elsevier. h) Illustration of the synthesis process of SA Ru-Co₃O₄/CC. i) Full discharge profiles of CC, Co₃O₄/CC and SA Ru-Co₃O₄/CC tested at 100 mA g⁻¹. j) Cycling performance comparison of CC, Co₃O₄/CC and SA Ru-Co₃O₄/CC at 200 mA g⁻¹. Reproduced with permission.^[207] Copyright 2021, Wiley-VCH.

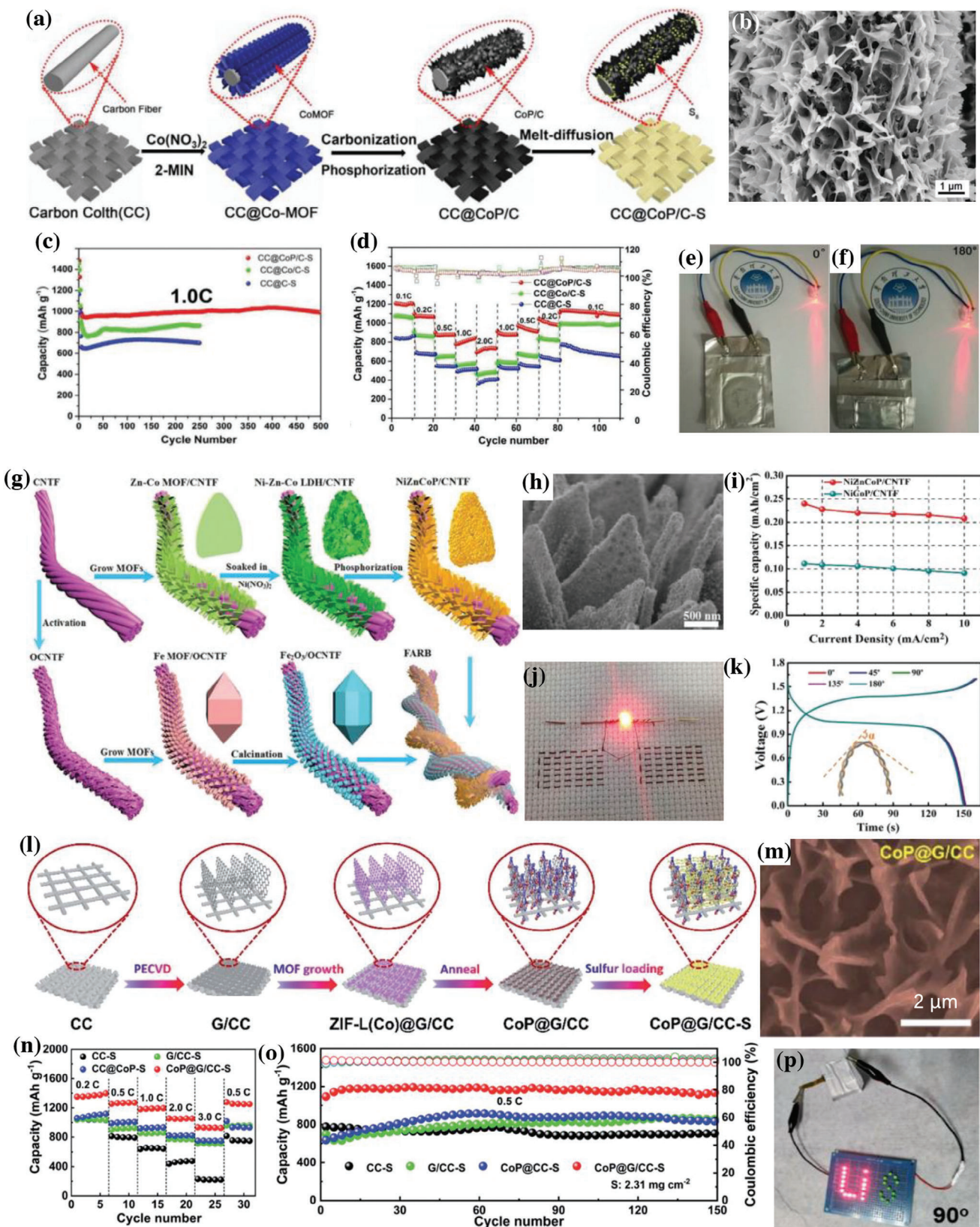


Figure 12. a) Schematic illustration of the detailed synthesis procedure for hybrid CC@CoP/C-S as flexible and self-supporting cathode for Li-S batteries. b) SEM image of CC@CoP/C-S. c) Long cyclic performance of the three sulfur cathodes (CC@C-S, CC@Co/C-S, and CC@CoP/C-S) at 1.0 C rates. d) Rate

are some concerns on their rapid faded rate capability and poor durability. To tackle the issues, Sun et al. particularly designed Cu-doped cobalt phosphide nanosheet arrays for flexible energy storage.^[209] Cu doping was achieved during the preparation of MOF nanoarrays, which turned into mesoporous Cu:CoP nanosheet arrays on CC after further oxidation and phosphorization process. The optimized Cu:CoP electrode delivered 3.3 times higher specific capacity and enhanced rate capability compared to the pristine CoP. To overcome the low surface area of CC and increase the mass loading of the active materials, secondary scaffolds have been introduced. For example, Jin et al. adopted PECVD method to construct vertical graphene (VG) network on CC. The cross-linked VG with an interconnected network enabled fast charge transfer, and offered extra space to accommodate the active materials.^[217] To fabricate cathode for Li-S batteries, Co-MOF derived CoP nanoarrays loaded with sulfur was prepared. The preparation process of CoP@G/CC-S is schematic illustrated in Figure 12l. The SEM image in Figure 12m revealed that the self-supported CoP@G/CC electrode possessed nanoarrays structures. When tested as cathode for Li-S batteries, the fabricated CoP@G/CC-S exhibited much higher specific capacity and better rate performance than that of CC-S or CC@CoP-S electrodes (Figure 12n). In terms of the cycling stability, CoP@G/CC-S exhibited outstanding stability after 150 cycles at high specific capacity (Figure 12o). The pouch cell based on CoP@G/CC-S cathode showed good mechanical flexibility and great potential in flexible energy storage application (Figure 12p).

4.6. Nitrogen-Doped Carbon Nanoarrays

In addition to various MOF-derived metal compounds, the application of MOF-derived nitrogen-doped carbon materials in the field of electrochemical energy storage is equally important and cannot be ignored due to the tailorable porous structure, high stability and excellent electrical conductivity.^[218–221] Moreover, both physical confinement and chemical adsorption of sulfur in nitrogen-doped carbons can effectively promote polysulfide immobilization, thus making nitrogen-doped carbon a perfect host for sulfur and good cathode for Li-S batteries.^[169,222] Though there are seldom reports on the direct use of MOF-derived nitrogen-doped carbon nanoarrays for flexible energy storage, N-doped carbon nanoarrays have been frequently used as a secondary substrate because carbon nanoarray structures possess enough interspace for the growth of active materials and help maintain the structural integrity.^[181] For example, Ren et al. adopted MOF-derived N-doped carbon nanowall arrays loaded with ultrathin MoS₂ nanosheets as anode for sodium ion battery.^[181] On one hand, N-doped porous carbon nanowall arrays improved the conductivity and maintained the structural in-

tegrity; on the other hand, N-doping-induced defects made them favorable for effective storage of sodium ions. When directly used as anode in sodium ion battery, the CC@CN electrode showed a capacity of 282 mA h g⁻¹ at 0.2 A g⁻¹. Cai et al. reported a Ni-MOF derived layered bamboo-like conductive carbon nitride (c-CN) material, which was applied as modified separator in Li-S battery and as flexible electrode in supercapacitor.^[168] Functional c-CN separator with excellent flexibility and uniformity was obtained through a simple vacuum filtration process. The porous architecture and large surface area of c-CN facilitated the enrichment of electron and ion pathways for electrochemical energy storage.

To simplify the preparation procedure, Guan et al. adopted “one for two strategy” that both the cathode and the anode materials of the flexible supercapacitor were derived from 2D Co-MOF nanoarrays.^[29] CC@NC anode was easily obtained via thermal treatment of Co-MOFs and followed by FeCl₃ etching process. The produced CC@NC anode showed near-rectangular CV curves and triangular GCD curves, indicating typical non-Faradaic double-layer behavior with good charge transfer. Moreover, it also exhibited superior rate performance and high specific capacitance of 321.9 F g⁻¹, outperforming many powder forms of porous carbon materials. Similarly, Chen et al. assembled flexible all-solid-state supercapacitors based on Co-MOF derived CoS₂ nanosheet array as cathode and nitrogen-doped carbon (CC@N-C) nanosheet array as anode.^[158] The all-solid-state supercapacitor based on CC@N-C anode not only achieved high energy density and robust cyclic stability, but also exhibited excellent flexibility under different deformation conditions and great operability under various thermal conditions.

4.7. Overviews

Most pristine MOF arrays are restrained from being utilized as electrode materials due to their poor electrical conductivity, but MOF-derived nanoarray structures with enhanced electrical conductivities can be readily produced via heat treatment of selected MOFs under controlled temperature, duration, and gas atmosphere. These MOF-derived nanoarray structures include but not limited to N-doped carbons, metal/metal oxide doped carbonaceous arrays, metal sulfide, metal selenide, metal nitride or metal phosphides embedded in porous carbon arrays and deposited on flexible substrates. These binder-free nanoarray structures exhibit efficient performance in various flexible electrochemical energy storage devices including supercapacitors and batteries, with great potential to power future wearable electronic devices. Some of the binder-free MOF based and MOF derived nanoarrays architectures as electrode materials for energy storage discussed above are listed in **Table 1**.

performance of the three cathodes (CC@C-S, CC@Co/C-S, and CC@CoP/C-S) at various current rates. e,f) Qualitative demonstration of the flexibility of Li/CC@CoP/C-S pouch cell powers the LED illumination at various folding angles. Reproduced with permission.^[215] Copyright 2019, Wiley-VCH. g) Schematic fabrication process of the twisted FARB device. h) SEM image of NiZnCoP nanosheet arrays. i) Specific capacities of the NiCoP/CNTF and NiZnCoP/CNTF electrodes at different current densities. j) The textiles of the FARBs device illuming a LED. k) GCD curves of the as-assembled FARBs bent at various angles at a current density of 2 mA cm⁻². Reproduced with permission.^[216] Copyright 2018, Wiley-VCH. l) Schematic illustration of the fabrication process of self-supported CoP@G/CC-S cathode. m) SEM image of CoP@G/CC. n) Rate capabilities of CC-S, G/CC-S, CoP@CC-S and CoP@G/CC-S cathodes. o) Cycling performance of CC-S, G/CC-S, CoP@CC-S and CoP@G/CC-S cathodes at 0.5 C. p) Digital photographs showing the mechanical flexibility of the pouch cell. Reproduced with permission.^[217] Copyright 2020, Royal Society of Chemistry.

Table 1. MOF based nanoarrays architectures as electrode materials for energy storage.

MOF Precursors	Nanoarrayed Electrode	Application	Specific Capacitance/ Capacities	Stability	Ref.
Cu-CAT	Cu-CAT	Supercapacitor	202 F g ⁻¹ at 0.5 A g ⁻¹	80% after 5000 cycles	[102]
Cu-CAT	4h-Cu-CAT-NWAs/PPy	Supercapacitor	484 mF cm ⁻² at 10 mV s ⁻¹	87% after 5000 cycles	[92]
V-MOF	V-MOF-48	Zn ion batteries	100.9 mAh cm ⁻³ at 0.1 A cm ⁻³	84.6% after 400 cycles	[103]
Ni-MOF	Ni-MOF-74@CNTF	Ni-Zn batteries	298.26 mAh cm ⁻³ at 0.5 A cm ⁻³	91.4% after 1000 cycles	[104]
CPO-27	CPO-27@250	Li ion batteries	834 mAh g ⁻¹ at 50 mA g ⁻¹	93% after 500 cycles	[109]
ZIF-8	ZnO@ZnO QDs/C NRAs	Li ion batteries	785 mAh g ⁻¹ at 500 mA g ⁻¹	89% after 100 cycles	[122]
ZIF-8	CC-ZnO@C-Zn	Zn-Co batteries	0.71 mAh cm ⁻² at 1 mA cm ⁻²	71.1% after 5000 cycles	[124]
ZIF-8	ZnO NRs/C@ (Ni ₃ Co) ₂ Se ₂ NSs	Supercapacitor	164.18 mAh g ⁻¹ at 1 A g ⁻¹	90.04% after 5000 cycles	[125]
ZIF-8	ZnO@C@CoNi-LDH	Supercapacitor	6.2578 F cm ⁻² at 2 mA cm ⁻²	95.01% after 10 000 cycles	[127]
ZIF-67	CCCH@NiCo-LDH NWAs@Au-CuO/Cu fibers	Supercapacitor	1970.1 mF cm ⁻² at 1.5 mA cm ⁻²	90.8% after 30 000 cycles	[129]
Mn-MOF	O _d -Mn ₃ O ₄ @C	Zn ion batteries	396.2 mAh g ⁻¹ at 0.2 A g ⁻¹	95.7% after 12 000 cycles	[141]
V-MOF	Ni-V ₂ O ₅ NWs@CNT	Zn ion batteries	90.3 mAh cm ⁻³ at 0.1 A cm ⁻³	89.8% after 10 000 cycles	[142]
Co-MOF	NC-Co ₃ O ₄ /CC	Zn-air batteries	387.2 mAh g ⁻¹ at 25 mA cm ⁻³	stably cycled for up to 60 cycles	[144]
Co-MOF	CC@Co ₃ O ₄	Supercapacitor	900 F g ⁻¹ at 10 A g ⁻¹	85.5% after 20 000 cycles	[29]
Co-MOF	CC@NiCo ₂ O ₄	Supercapacitor	1055.3 F g ⁻¹ at 2.5 mA cm ⁻²	86.7% after 20 000 cycles	[146]
Co-MOF	ZnCo ₂ O ₄ @NC NWAs	Supercapacitor	2.244 F cm ⁻² at 2 mA cm ⁻²	99.37% after 10 000 cycles	[145]
Co-MOF	NiCo-DH	Ni-Zn batteries	303.6 mAh g ⁻¹ at 2 mA cm ⁻²	73% after 850 cycles	[150]
Co-MOF	Co(VO ₃) ₂ Co(OH) ₂	Supercapacitor	522 mF cm ⁻² at 0.5 mA cm ⁻²	90% after 15 000 cycles	[154]
Co-MOF	CC/MOFC/MnO ₂	Supercapacitor	651.7 mF cm ⁻² at 1.0 mA cm ⁻²	50% after 5000 cycles	[155]
Co-MOF	CC/CW/Fe ₃ O ₄ @C	Supercapacitor	463 F g ⁻¹ at 1 A g ⁻¹	92.8% after 10 000 cycles	[157]
Co-MOF	Co ₃ O ₄ @NiCo ₂ O ₄	Li-O ₂ batteries	10 645 mAh g ⁻¹ at 100 mA g ⁻¹	stably cycled for 225 cycles	[149]
Zn-MOF	CF@NiCoZn-LDH/Co ₃ S ₈ -QD	Supercapacitor	350.6 mAh g ⁻¹ at 1 A g ⁻¹	95.3% after 8000 cycles	[172]
Zn-MOF	CF@NiCoZn-S/NiCo ₂ S ₄	Supercapacitor	194 mAh g ⁻¹ at 1 A g ⁻¹	70.1% after 10 000 cycles	[174]
ZIF-67	NiCo ₂ S ₄ @CC	Supercapacitor	879.6 F g ⁻¹ at 1 A g ⁻¹	98.39% after 10 000 cycles	[176]
Co-MOF	CC@CN@MoS ₂	Na ion batteries	653.9 mAh g ⁻¹ at 0.2 A g ⁻¹	75.3% after 1000 cycles	[181]
Co-MOF	P-CoS ₂ @P, S, N-C	Supercapacitor	689 C g ⁻¹ at 2 A g ⁻¹	95.5% after 5000 cycles	[179]
Co-MOF	P-doped CoSe ₂ /N-C	Zn-air batteries	None	stably cycled for up to 80 cycles	[192]
Co-MOF	Co _{0.85} Se/NC-S	Li-S batteries	1361 mAh g ⁻¹ at 0.1 C	83.87% after 400 cycles	[193]
ZIF-67	Co ₃ O ₄ Se ₂ @C/CC	Alkaline Zn batteries	7.42 mAh cm ⁻² at 10 mA cm ⁻²	72.4% after 10 000 cycles	[194]
Co-MOF	NC-Co/CoN _x	Zn-air batteries	41.5 mW cm ⁻³ at 96.6 mA cm ⁻³	stably cycled for up to 1200 cycles	[198]
Co-MOF	Ni-doped Co-Co ₂ N	Supercapacitor	361.93 C g ⁻¹ at 2 mA cm ⁻²	82.4% after 5000 cycles	[147]
Co-MOF	CC/CW/p-VN@C	Supercapacitor	604.8 F g ⁻¹ at 1 A g ⁻¹	90.5% after 10 000 cycles	[199]
Co/Fe-MOF	Fe-CoN ₄ @N-C	Zn-air batteries	806 mAh g ⁻¹ at 5 mA cm ⁻²	stably cycled for up to 220 cycles	[200]
Co-MOF	NC-Co SAC	Zn-air batteries	0.9 mW cm ⁻³ at 31.0 mA cm ⁻²	stably cycled for up to 125 cycles	[205]
Co-MOF	CC@CoP/C-S	Li-S batteries	1535 mAh g ⁻¹ at 0.1 C	96.9% after 500 cycles	[215]
Co-MOF	CoP/NC	Li-S batteries	1482 mAh g ⁻¹ at 0.1 C	81.6% after 560 cycles	[213]
Zn-Co MOF	NiZnCoP@CNTF	NiCo-Fe batteries	0.24 mAh cm ⁻² at 1 mA cm ⁻²	92.1% after 8000 cycles	[216]
Co-MOF	CoP@G/CC-S	Li-S batteries	8.81 mAh cm ⁻² at 0.05 C	85% after 500 cycles	[217]

5. Summary and Perspective

In summary, recent research progress in the applications of MOF-based and MOF-derived nanoarrays (metal oxides, sulfides, selenides, nitrides, phosphides and N-doped carbons, etc.) as binder-free nanostructured electrodes in flexible energy storage has been reviewed. Fabrication methods and electrochemical performance of these nanoarray electrodes are discussed and overviewed. Moreover, the commonly used flexible substrates (carbon cloth, electrospinning nanofiber, paper, MXene film, metal foams, etc.) are also systematically overviewed, and each

type of substrates has been analyzed and compared in terms of chemical stability, flexibility, conductivity, cost and capacitance contribution. Despite great progress has been achieved in binder-free MOF-based and MOF-derived nanoarrays for flexible energy storage, there is still a long way to go to realize the practical utilizations. Further extensive researches are needed to develop high performance flexible energy storage devices, ranging from substrate fabrication, active materials preparation to device assembling. Some challenges and perspectives are listed as follows.

First of all, design and preparation of new flexible substrate with low cost, good conductivity, robust mechanical stability, as

well as capacitance contribution to achieve high performance for flexible energy storage devices is highly desirable. In this regard, the development of conductive polymers with excellent properties for electrochemical energy storage will be very attractive. Most of conductive polymers are cheap and possess good mechanical flexibility and elasticity, which are the prerequisites to be an ideal flexible substrate. Moreover, it is easy to modulate and regulate the active groups in conductive polymers via various chemical reactions, which can benefit the control of the hydrophilic and hydrophobic nature of the substrates, and adjust the adhesion force between the active materials and the substrates, thus, to well maintain the structural stability of the electrode in flexible energy storage devices.

Second, design and synthesis of conductive MOF nanoarrays are very promising strategies to achieve fast energy storage in electrochemical devices. Though some conductive MOFs have been successfully synthesized and explored for potential applications in energy storage and conversion in the past years,^[223–225] more and better conductive MOFs will be synthesized by tuning the coordination and composition of ligands or introducing mixed-valence metal ions in the future. Exploring multidentate ligands with strong π -conjugated planners or π - π stacks would enhance the conductivity of the related MOFs. Moreover, excavating organic ligands with redox-active sites as well as the formation of infinite metal-sulfur chains would also be helpful to increase the electrical conductivity of MOFs. In addition, making use of machine learning to guide MOF synthesis toward targeted structures and properties, such as structurally stable MOFs with larger surface area and more active sites, could have great potential in producing conductive MOFs nanoarrays meeting the prerequisites of electrodes for flexible electrochemical energy storage and conversion devices.

Third, though a variety of MOF-based or MOF-derived nanoarrays have been synthesized, the growth mechanism of the nanoarray is not clear. It is therefore valuable to investigate and optimize the different synthesis parameters including temperature, synthesis duration, the types and the amounts of precursors and solvents etc. that influence the microstructures and morphologies of nanoarrays. Another challenge is how to effectively control the structure evolution to avoid the collapse of nanoarrays during long-term charge–discharge process. In this respect, understanding of the reaction mechanisms and structure evolution of nanoarray electrodes through state-of-art in situ characterization technologies including in situ Raman etc. is particularly desirable. In addition, exploration of electrochemical dynamics of interface between electrolyte and electrode is also highly valuable.

It is expected that this review will inspire valuable insight and trigger more creative research in the development of binder-free MOF-based and MOF derived nanoarrays for flexible electrochemical energy storage, which may flourish and bring forward these nanostructured arrays to be practical utilized in future wearable electronic devices.

Acknowledgements

This work was supported by Ph.D. Research Startup Fund (BK202217) in Hubei University of Automotive Technology. Financial support by the Leverhulme Trust (RPG-2018–320) and the Royal Society (IEC\NSFC\201121) is also acknowledged.

Conflict of Interest

The authors declare no conflict of interest.

Keywords

electrodes, electrochemical energy storage, metal–organic frameworks, metal–organic framework derivatives, nanoarrays

Received: July 10, 2023

Revised: October 9, 2023

Published online:

- [1] Z. W. Seh, J. Kibsgaard, C. F. Dickens, I. Chorkendorff, J. K. Nørskov, T. F. Jaramillo, *Science* **2017**, *355*, 146.
- [2] N. Zhang, X. Chen, M. Yu, Z. Niu, F. Cheng, J. Chen, *Chem. Soc. Rev.* **2020**, *49*, 4203.
- [3] C. Choi, D. S. Ashby, D. M. Butts, R. H. DeBlock, Q. Wei, J. Lau, B. Dunn, *Nat. Rev. Mater.* **2019**, *5*, 5.
- [4] J. He, C. Lu, H. Jiang, F. Han, X. Shi, J. Wu, L. Wang, T. Chen, J. Wang, Y. Zhang, H. Yang, G. Zhang, X. Sun, B. Wang, P. Chen, Y. Wang, Y. Xia, H. Peng, *Nature* **2021**, *597*, 57.
- [5] F. Qi, Z. Sun, X. Fan, Z. Wang, Y. Shi, G. Hu, F. Li, *Adv. Energy Mater.* **2021**, *11*, 2100387.
- [6] Y. Wang, Q. Cao, C. Guan, C. Cheng, *Small* **2020**, *16*, 2002902.
- [7] T. Wang, Z. Tian, Z. You, Z. Li, H. Cheng, W. Li, Y. Yang, Y. Zhou, Q. Zhong, Y. Lai, *Energy Storage Mater.* **2022**, *45*, 24.
- [8] Q. Cao, H. Gao, Y. Gao, J. Yang, C. Li, J. Pu, J. Du, J. Yang, D. Cai, Z. Pan, C. Guan, W. Huang, *Adv. Funct. Mater.* **2021**, *31*, 2103922.
- [9] E. Pomerantseva, F. Bonaccorso, X. Feng, Y. Cui, Y. Gogotsi, *Science* **2019**, *366*, 969.
- [10] L. Zhang, X. Qin, S. Zhao, A. Wang, J. Luo, Z. L. Wang, F. Kang, Z. Lin, B. Li, *Adv. Mater.* **2020**, *32*, 1908445.
- [11] X. Zhao, K. Tao, L. Han, *Nanoscale* **2022**, *14*, 2155.
- [12] J. Cui, P. Yin, A. Xu, B. Jin, Z. Li, M. Shao, *Nano Energy* **2021**, *93*, 106837.
- [13] J. Tan, W. Zhu, Q. Gui, Y. Li, J. Liu, *Adv. Funct. Mater.* **2021**, *31*, 2101027.
- [14] X. Cao, C. Tan, M. Sindoro, H. Zhang, *Chem. Soc. Rev.* **2017**, *46*, 2660.
- [15] H. Zhang, X. Liu, Y. Wu, C. Guan, A. K. Cheetham, J. Wang, *Chem. Commun.* **2018**, *54*, 5268.
- [16] J. Ren, Y. Huang, H. Zhu, B. Zhang, H. Zhu, S. Shen, G. Tan, F. Wu, H. He, S. Lan, X. Xia, Q. Liu, *Carbon Energy* **2020**, *2*, 176.
- [17] H. B. Wu, X. W. Lou, *Sci. Adv.* **2017**, *3*, eaap9252.
- [18] H. Furukawa, K. E. Cordova, M. O'Keeffe, O. M. Yaghi, *Science* **2013**, *341*, 1230444.
- [19] H. Daglar, H. C. Gulbalkan, G. Avcı, G. O. Aksu, O. F. Altundal, C. Altintas, I. Erucar, S. Keskin, *Angew. Chem., Int. Ed.* **2021**, *60*, 7828.
- [20] H. Daglar, S. Keskin, *Coord. Chem. Rev.* **2020**, *422*, 213470.
- [21] M. X. Wu, Y. W. Yang, *Adv. Mater.* **2017**, *29*, 1606134.
- [22] M.-S. Yao, W.-H. Li, G. Xu, *Coord. Chem. Rev.* **2021**, *426*, 213479.
- [23] X. Zhou, H. Jin, B. Y. Xia, K. Davey, Y. Zheng, S. Z. Qiao, *Adv. Mater.* **2021**, *33*, 2104341.
- [24] T. Qiu, Z. Liang, W. Guo, H. Tabassum, S. Gao, R. Zou, *ACS Energy Lett.* **2020**, *5*, 520.
- [25] K. Shen, Z. Lei, X. Chen, L. Liu, B. Chen, *Science* **2018**, *359*, 206.
- [26] J.-B. Lin, T. T. Nguyen, R. Vaidyanathan, J. Burner, J. M. Taylor, H. Durekova, F. Akhtar, R. K. Mah, O. Ghaffari-Nik, S. Marx, N. Fylstra, S. S. Iremonger, K. W. Dawson, P. Sarkar, P. Hovington, A. Rajendran, T. K. Woo, G. K. H. Shimizu, *Science* **2021**, *374*, 1464.

- [27] M. Z. Hussain, Z. Yang, Z. Huang, Q. Jia, Y. Zhu, Y. Xia, *Adv. Sci.* **2021**, *8*, 2100625.
- [28] B. Chen, Z. Yang, Q. Jia, R. J. Ball, Y. Zhu, Y. Xia, *Mater. Sci. Eng. R* **2023**, *152*, 100714.
- [29] C. Guan, W. Zhao, Y. Hu, Z. Lai, X. Li, S. Sun, H. Zhang, A. K. Cheetham, J. Wang, *Nanoscale Horiz.* **2017**, *2*, 99.
- [30] A. I. Khan, A. Daus, R. Islam, K. M. Neilson, H. R. Lee, H.-S. P. Wong, E. Pop, *Science* **2021**, *373*, 1243.
- [31] Z. X. Cai, Z. L. Wang, J. Kim, Y. Yamauchi, *Adv. Mater.* **2019**, *31*, 1804903.
- [32] Z. Liu, F. Mo, H. Li, M. Zhu, Z. Wang, G. Liang, C. Zhi, *Small Methods* **2018**, *2*, 1800124.
- [33] W. Liu, R. Yin, X. Xu, L. Zhang, W. Shi, X. Cao, *Adv. Sci.* **2019**, *6*, 1802373.
- [34] J. Liu, X. Song, T. Zhang, S. Liu, H. Wen, L. Chen, *Angew. Chem., Int. Ed.* **2020**, *60*, 5612.
- [35] W. Xia, A. Mahmood, R. Zou, Q. Xu, *Energy Environ. Sci.* **2015**, *8*, 1837.
- [36] S. Z. Yuqi Xue, H. Xue, H. Pang, *J. Mater. Chem. A* **2019**, *7*, 7301.
- [37] Y. Li, Y. Xu, W. Yang, W. Shen, H. Xue, H. Pang, *Small* **2018**, *14*, 1704435.
- [38] S. Dang, Q.-L. Zhu, Q. Xu, *Nat. Rev. Mater.* **2017**, *3*, 17075.
- [39] B. He, Q. Zhang, Z. Pan, L. Li, C. Li, Y. Ling, Z. Wang, M. Chen, Z. Wang, Y. Yao, Q. Li, L. Sun, J. Wang, L. Wei, *Chem. Rev.* **2022**, *122*, 10087.
- [40] L. Li, W. Liu, H. Dong, Q. Gui, Z. Hu, Y. Li, J. Liu, *Adv. Mater.* **2021**, *33*, 2004959.
- [41] C. Zhu, H. Wang, C. Guan, *Nanoscale Horiz.* **2020**, *5*, 1188.
- [42] P. Yang, Y. Ding, Z. Lin, Z. Chen, Y. Li, P. Qiang, M. Ebrahimi, W. Mai, C. P. Wong, Z. L. Wang, *Nano Lett.* **2014**, *14*, 731.
- [43] C. Guan, W. Zhao, Y. Hu, Q. Ke, X. Li, H. Zhang, J. Wang, *Adv. Energy Mater.* **2016**, *6*, 1601034.
- [44] X. Liu, W. Xu, D. Zheng, Z. Li, Y. Zeng, X. Lu, *J. Mater. Chem. A* **2020**, *8*, 17938.
- [45] F. Han, J. Xu, J. Zhou, J. Tang, W. Tang, *Nanoscale* **2019**, *11*, 12477.
- [46] L. Wang, H. Yang, X. Liu, R. Zeng, M. Li, Y. Huang, X. Hu, *Angew. Chem., Int. Ed.* **2017**, *56*, 1105.
- [47] K. A. Owusu, L. Qu, J. Li, Z. Wang, K. Zhao, C. Yang, K. M. Hercule, C. Lin, C. Shi, Q. Wei, L. Zhou, L. Mai, *Nat. Commun.* **2017**, *8*, 14264.
- [48] L.-F. Chen, Z.-Y. Yu, J.-J. Wang, Q.-X. Li, Z.-Q. Tan, Y.-W. Zhu, S.-H. Yu, *Nano Energy* **2015**, *11*, 119.
- [49] J. Shang, Q. Huang, L. Wang, Y. Yang, P. Li, Z. Zheng, *Adv. Mater.* **2020**, *32*, 1907088.
- [50] J. Zhao, H. Cheng, H. Li, Y.-J. Wang, Q. Jiang, L. Yang, A. Meng, J. Huang, C. Sun, H. Li, Z. Li, J. Zhang, *J. Mater. Chem. A* **2021**, *9*, 20794.
- [51] H. Zhang, Y. Lv, X. Wu, J. Guo, D. Jia, *Chem. Eng. J.* **2021**, *431*, 133233.
- [52] S. Chen, J. Zhang, Z. Wang, L. Nie, X. Hu, Y. Yu, W. Liu, *Nano Lett.* **2021**, *21*, 5285.
- [53] S. Liu, L. Kang, J. Hu, E. Jung, J. Henzie, A. Alowasheer, J. Zhang, L. Miao, Y. Yamauchi, S. C. Jun, *Small* **2021**, *18*, 2104507.
- [54] M. Nakayama, K. Komine, D. Inohara, *J. Electrochem. Soc.* **2016**, *163*, A2428.
- [55] H. Wang, J. Deng, C. Xu, Y. Chen, F. Xu, J. Wang, Y. Wang, *Energy Storage Mater.* **2017**, *7*, 216.
- [56] G. Wang, H. Wang, X. Lu, Y. Ling, M. Yu, T. Zhai, Y. Tong, Y. Li, *Adv. Mater.* **2014**, *26*, 2676.
- [57] T. Qin, H. Chen, Y. Zhang, X. Chen, L. Liu, D. Yan, S. Ma, J. Hou, F. Yu, S. Peng, *J. Power Sources* **2019**, *431*, 232.
- [58] Y. Han, Y. Lu, S. Shen, Y. Zhong, S. Liu, X. Xia, Y. Tong, X. Lu, *Adv. Funct. Mater.* **2019**, *29*, 1806329.
- [59] Z. Xue, X. Li, Q. Liu, M. Cai, K. Liu, M. Liu, Z. Ke, X. Liu, G. Li, *Adv. Mater.* **2019**, *31*, 1900430.
- [60] D. Ji, L. Fan, L. Li, S. Peng, D. Yu, J. Song, S. Ramakrishna, S. Guo, *Adv. Mater.* **2019**, *31*, 1808267.
- [61] B. Li, K. Igawa, J. Chai, Y. Chen, Y. Wang, D. W. Fam, N. N. Tham, T. An, T. Konno, A. Sng, Z. Liu, H. Zhang, Y. Zong, *Energy Storage Mater.* **2020**, *25*, 137.
- [62] A. Abdul Razzaq, X. Yuan, Y. Chen, J. Hu, Q. Mu, Y. Ma, X. Zhao, L. Miao, J.-H. Ahn, Y. Peng, Z. Deng, *J. Mater. Chem. A* **2020**, *8*, 1298.
- [63] L. Yang, X. Zhang, L. Yu, J. Hou, Z. Zhou, R. Lv, *Adv. Mater.* **2021**, *33*, 2105410.
- [64] M. Du, D. Song, A. Huang, R. Chen, D. Jin, K. Rui, C. Zhang, J. Zhu, W. Huang, *Angew. Chem. Int. Ed.* **2019**, *58*, 5307.
- [65] Y. Yan, X. Liu, J. Yan, C. Guan, J. Wang, *Energy Environ. Mater.* **2020**, *4*, 502.
- [66] Z. Li, J. Bu, C. Zhang, L. Cheng, D. Pan, Z. Chen, M. Wu, *New J. Chem.* **2021**, *45*, 10672.
- [67] T. G. Yun, M. Park, D. H. Kim, D. Kim, J. Y. Cheong, J. G. Bae, S. M. Han, I. D. Kim, *ACS Nano* **2019**, *13*, 3141.
- [68] Q. Xu, C. Wu, X. Sun, H. Liu, H. Yang, H. Hu, M. Wu, *Nanoscale* **2021**, *13*, 18391.
- [69] M. B. Poudel, H. J. Kim, *Chem. Eng. J.* **2022**, *429*, 132345.
- [70] M. Yao, C. Guo, Y. Zhang, X. Zhao, Y. Wang, *J. Mater. Chem. C* **2022**, *10*, 542.
- [71] M. Liu, X. Li, C. Shao, C. Han, Y. Liu, X. Li, X. Ma, F. Chen, Y. Liu, *Energy Storage Mater.* **2022**, *44*, 250.
- [72] B. G. Kim, D. W. Kang, G. Park, S. H. Park, S.-M. Lee, J. W. Choi, *Chem. Eng. J.* **2021**, *422*, 130017.
- [73] Y. Yan, J. Yan, X. Gong, X. Tang, X. Xu, T. Meng, F. Bu, D. Cai, Z. Zhang, G. Nie, H. Zhang, *Chem. Eng. J.* **2022**, *433*, 133580.
- [74] Y. Z. Zhang, Y. Wang, T. Cheng, W. Y. Lai, H. Pang, W. Huang, *Chem. Soc. Rev.* **2015**, *44*, 5181.
- [75] Y. Chen, K. Cai, C. Liu, H. Song, X. Yang, *Adv. Energy Mater.* **2017**, *7*, 1701247.
- [76] A. Chebil, V. Mazzaracchio, S. Cinti, F. Arduini, C. Dridi, *J. Energy Storage* **2021**, *33*, 102107.
- [77] Z. Chang, A. Huang, X. An, X. Qian, *Carbohydr. Polym.* **2020**, *244*, 116442.
- [78] G. Zheng, L. Hu, H. Wu, X. Xie, Y. Cui, *Energy Environ. Sci.* **2011**, *4*, 3368.
- [79] K. Li, X. Liu, S. Chen, W. Pan, J. Zhang, *J. Energy Chem.* **2019**, *32*, 166.
- [80] D. Mandal, P. Routh, A. K. Mahato, A. K. Nandi, *J. Mater. Chem. A* **2019**, *7*, 17547.
- [81] L. Zhang, X. Yu, P. Zhu, F. Zhou, G. Li, R. Sun, C.-P. Wong, *Sustain. Energy Fuels* **2018**, *2*, 147.
- [82] X. Wu, M. Zhang, T. Song, H. Mou, Z. Xiang, H. Qi, *ACS Appl. Mater. Interfaces* **2020**, *12*, 13096.
- [83] M. Bharti, A. Singh, B. P. Singh, S. R. Dhakate, G. Saini, S. Bhattacharya, A. K. Debnath, K. P. Muthe, D. K. Aswal, *J. Power Sources* **2020**, *449*, 227493.
- [84] B. Yang, C. Hao, F. Wen, B. Wang, C. Mu, J. Xiang, L. Li, B. Xu, Z. Zhao, Z. Liu, Y. Tian, *ACS Appl. Mater. Interfaces* **2017**, *9*, 44478.
- [85] J. Yun, Y. Lim, H. Lee, G. Lee, H. Park, S. Y. Hong, S. W. Jin, Y. H. Lee, S.-S. Lee, J. S. Ha, *Adv. Funct. Mater.* **2017**, *27*, 1700135.
- [86] R. Guo, J. Chen, B. Yang, L. Liu, L. Su, B. Shen, X. Yan, *Adv. Funct. Mater.* **2017**, *27*, 1702394.
- [87] P. Sundriyal, S. Bhattacharya, *ACS Appl. Mater. Interfaces* **2017**, *9*, 38507.
- [88] J. Chen, Y. Liu, A. I. Minett, C. Lynam, J. Wang, G. G. Wallace, *Chem. Mater.* **2007**, *19*, 3595.
- [89] C. Hwang, W. J. Song, J. G. Han, S. Bae, G. Song, N. S. Choi, S. Park, H. K. Song, *Adv. Mater.* **2018**, *30*, 1705445.
- [90] W. Liu, Z. Chen, G. Zhou, Y. Sun, H. R. Lee, C. Liu, H. Yao, Z. Bao, Y. Cui, *Adv. Mater.* **2016**, *28*, 3578.
- [91] K. Qi, Y. Qiu, Z. Chen, X. Guo, *Corros. Sci.* **2014**, *80*, 318.

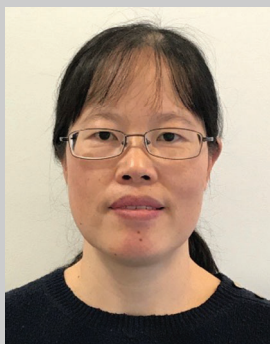
- [92] R. Hou, M. Miao, Q. Wang, T. Yue, H. Liu, H. S. Park, K. Qi, B. Y. Xia, *Adv. Energy Mater.* **2019**, *10*, 1901892.
- [93] T. Yue, R. Hou, X. Liu, K. Qi, Z. Chen, Y. Qiu, X. Guo, B. Y. Xia, *ACS Appl. Energy Mater.* **2020**, *3*, 11920.
- [94] Z. Fan, C. Wei, L. Yu, Z. Xia, J. Cai, Z. Tian, G. Zou, S. X. Dou, J. Sun, *ACS Nano* **2020**, *14*, 867.
- [95] L. Gao, W. Bao, A. V. Kuklin, S. Mei, H. Zhang, H. Agren, *Adv. Mater.* **2021**, *33*, 2004129.
- [96] S. Wang, Q. Wang, W. Zeng, M. Wang, L. Ruan, Y. Ma, *Nano-Micro Lett.* **2019**, *11*, 70.
- [97] G. S. Gund, J. H. Park, R. Harpalsinh, M. Kota, J. H. Shin, T.-i. Kim, Y. Gogotsi, H. S. Park, *Joule* **2019**, *3*, 164.
- [98] V. Egorov, C. O'Dwyer, *Curr. Opin. Electrochem.* **2020**, *21*, 201.
- [99] R. Choudhury, J. Wild, Y. Yang, *Joule* **2021**, *5*, 1301.
- [100] D. Sheberla, J. C. Bachman, J. S. Elias, C. J. Sun, Y. Shao-Horn, M. Dinca, *Nat. Mater.* **2017**, *16*, 220.
- [101] D. Feng, T. Lei, M. R. Lukatskaya, J. Park, Z. Huang, M. Lee, L. Shaw, S. Chen, A. A. Yakovenko, A. Kulkarni, J. Xiao, K. Fredrickson, J. B. Tok, X. Zou, Y. Cui, Z. Bao, *Nat. Energy* **2018**, *3*, 30.
- [102] W.-H. Li, K. Ding, H.-R. Tian, M.-S. Yao, B. Nath, W.-H. Deng, Y. Wang, G. Xu, *Adv. Funct. Mater.* **2017**, *27*, 1702067.
- [103] B. He, Q. Zhang, P. Man, Z. Zhou, C. Li, Q. Li, L. Xie, X. Wang, H. Pang, Y. Yao, *Nano Energy* **2019**, *64*, 103935.
- [104] P. Man, B. He, Q. Zhang, Z. Zhou, C. Li, Q. Li, L. Wei, Y. Yao, *J. Mater. Chem. A* **2019**, *7*, 27217.
- [105] M. L. Aubrey, B. M. Wiers, S. C. Andrews, T. Sakurai, S. E. Reyes-Lillo, S. M. Hamed, C. J. Yu, L. E. Darago, J. A. Mason, J. O. Baeg, F. Grandjean, G. J. Long, S. Seki, J. B. Neaton, P. Yang, J. R. Long, *Nat. Mater.* **2018**, *17*, 625.
- [106] L. E. Darago, M. L. Aubrey, C. J. Yu, M. I. Gonzalez, J. R. Long, *J. Am. Chem. Soc.* **2015**, *137*, 15703.
- [107] L. S. Xie, L. Sun, R. Wan, S. S. Park, J. A. DeGayner, C. H. Hendon, M. Dincă, *J. Am. Chem. Soc.* **2018**, *140*, 7411.
- [108] L. Sun, M. G. Campbell, M. Dinca, *Angew. Chem., Int. Ed.* **2016**, *55*, 3566.
- [109] D. Zhou, J. Ni, L. Li, *Nano Energy* **2019**, *57*, 711.
- [110] M. Xu, X. Wang, K. Ouyang, Z. Xu, *Energy Fuels* **2021**, *35*, 19818.
- [111] R. Zhao, Z. Liang, R. Zou, Q. Xu, *Joule* **2018**, *2*, 2235.
- [112] G. J. H. Lim, *Electrochim. Acta* **2018**, *291*, 177.
- [113] H. Xu, X. Hu, H. Yang, Y. Sun, C. Hu, Y. Huang, *Adv. Energy Mater.* **2015**, *5*, 1401882.
- [114] F. Zheng, G. Xia, Y. Yang, Q. Chen, *Nanoscale* **2015**, *7*, 9637.
- [115] W. Zhou, Y. Tang, X. Zhang, S. Zhang, H. Xue, H. Pang, *Coord. Chem. Rev.* **2023**, *477*, 214949.
- [116] J. Zhao, H. Li, C. Li, Q. Zhang, J. Sun, X. Wang, J. Guo, L. Xie, J. Xie, B. He, Z. Zhou, C. Lu, W. Lu, G. Zhu, Y. Yao, *Nano Energy* **2018**, *45*, 420.
- [117] Z. Pan, J. Zhong, Q. Zhang, J. Yang, Y. Qiu, X. Ding, K. Nie, H. Yuan, K. Feng, X. Wang, G. Xu, W. Li, Y. Yao, Q. Li, M. Liu, Y. Zhang, *Adv. Energy Mater.* **2018**, *8*, 1702946.
- [118] M. D. Hossain, Z. Liu, M. Zhuang, X. Yan, G.-L. Xu, C. A. Gadre, A. Tyagi, I. H. Abidi, C.-J. Sun, H. Wong, A. Guda, Y. Hao, X. Pan, K. Amine, Z. Luo, *Adv. Energy Mater.* **2019**, *9*, 1803689.
- [119] Q. Li, Q. Zhang, C. Liu, J. Sun, J. Guo, J. Zhang, Z. Zhou, B. He, Z. Pan, Y. Yao, *J. Mater. Chem. A* **2019**, *7*, 520.
- [120] J. Yao, H. Wan, C. Chen, J. Ji, N. Wang, Z. Zheng, J. Duan, X. Wang, G. Ma, L. Tao, H. Wang, J. Zhang, H. Wang, *Nanomicro. Lett.* **2021**, *13*, 167.
- [121] Q. Li, S. Jing, Z. Yong, Q. Zhang, C. Liu, K. Zhu, Y. Feng, W. Gong, Y. Yao, *Energy Storage Mater.* **2021**, *42*, 815.
- [122] G. Zhang, S. Hou, H. Zhang, W. Zeng, F. Yan, C. C. Li, H. Duan, *Adv. Mater.* **2015**, *27*, 2400.
- [123] Z. Tang, G. Zhang, H. Zhang, L. Wang, H. Shi, D. Wei, H. Duan, *Energy Storage Mater.* **2018**, *10*, 75.
- [124] M. Li, J. Meng, Q. Li, M. Huang, X. Liu, K. A. Owusu, Z. Liu, L. Mai, *Adv. Funct. Mater.* **2018**, *28*, 1802016.
- [125] W. Liu, F. Zhu, B. Ge, L. Sun, Y. Liu, W. Shi, *Chem. Eng. J.* **2022**, *427*, 130788.
- [126] Q. Gan, K. Zhao, S. Liu, Z. He, *J. Mater. Sci.* **2017**, *52*, 7768.
- [127] Q. Yang, Z. Li, R. Zhang, L. Zhou, M. Shao, M. Wei, *Nano Energy* **2017**, *41*, 408.
- [128] S. Dai, Y. Yuan, J. Yu, J. Tang, J. Zhou, W. Tang, *Nanoscale* **2018**, *10*, 15454.
- [129] Y. Guo, X. Hong, Y. Wang, Q. Li, J. Meng, R. Dai, X. Liu, L. He, L. Mai, *Adv. Funct. Mater.* **2019**, *29*, 1809004.
- [130] G. Li, H. Cai, X. Li, J. Zhang, D. Zhang, Y. Yang, J. Xiong, *ACS Appl. Mater. Interfaces* **2019**, *11*, 37675.
- [131] Y. Chong, Z. Pan, M. Su, X. Yang, D. Ye, Y. Qiu, *Electrochim. Acta* **2020**, *363*, 137264.
- [132] X. He, Y. Zhao, R. Chen, H. Zhang, J. Liu, Q. Liu, D. Song, R. Li, J. Wang, *ACS Sustainable Chem. Eng.* **2018**, *6*, 14945.
- [133] C. Zhou, Y. Zhang, Y. Li, J. Liu, *Nano Lett.* **2013**, *13*, 2078.
- [134] W. Zeng, G. Zhang, X. Wu, K. Zhang, H. Zhang, S. Hou, C. Li, T. Wang, H. Duan, *J. Mater. Chem. A* **2015**, *3*, 24033.
- [135] I. Hussain, M. Z. Ansari, M. Ahmad, A. Ali, T. Nawaz, T. Hussain, C. Lamiel, M. Sufyan Javed, X. Chen, M. Sajjad, T. Kaewmaraya, K. Khan, K. Zhang, *Adv. Funct. Mater.* **2023**, *33*, 2302888.
- [136] C. Zhu, Y. Ma, W. Zang, C. Guan, X. Liu, S. J. Pennycook, J. Wang, W. Huang, *Chem. Eng. J.* **2019**, *369*, 988.
- [137] G. Fang, J. Zhou, C. Liang, A. Pan, C. Zhang, Y. Tang, X. Tan, J. Liu, S. Liang, *Nano Energy* **2016**, *26*, 57.
- [138] X. Wang, Z. Liao, Y. Fu, C. Neumann, A. Turchanin, G. Nam, E. Zschech, J. Cho, J. Zhang, X. Feng, *Energy Storage Mater.* **2020**, *26*, 157.
- [139] Y. Ma, J. He, Z. Kou, A. M. Elshahawy, Y. Hu, C. Guan, X. Li, J. Wang, *Adv. Mater. Interfaces* **2018**, *5*, 1800222.
- [140] S. Kamari Kaverlavani, L. Abbasi, Y. K. Mishra, S. Y. Hosseini, M. N. Liavali, S. E. Moosavifard, *ACS Sustainable Chem. Eng.* **2022**, *10*, 13310.
- [141] Q. Tan, X. Li, B. Zhang, X. Chen, Y. Tian, H. Wan, L. Zhang, L. Miao, C. Wang, Y. Gan, J. Jiang, Y. Wang, H. Wang, *Adv. Energy Mater.* **2020**, *10*, 2001050.
- [142] T. Li, Q. Xu, M. Waqar, H. Yang, W. Gong, J. Yang, J. Zhong, Z. Liu, *Energy Storage Mater.* **2023**, *55*, 64.
- [143] D. Ji, L. Fan, L. Li, N. Mao, X. Qin, S. Peng, S. Ramakrishna, *Carbon* **2019**, *142*, 379.
- [144] C. Guan, A. Sumboja, H. Wu, W. Ren, X. Liu, H. Zhang, Z. Liu, C. Cheng, S. J. Pennycook, *J. Wang, Adv. Mater.* **2017**, *29*, 1704117.
- [145] D. Kong, Y. Wang, S. Huang, J. Hu, Y. V. Lim, B. Liu, S. Fan, Y. Shi, H. Y. Yang, *Energy Storage Mater.* **2019**, *23*, 653.
- [146] C. Guan, X. Liu, W. Ren, X. Li, C. Cheng, J. Wang, *Adv. Energy Mater.* **2017**, *7*, 1602391.
- [147] X. Liu, W. Zang, C. Guan, L. Zhang, Y. Qian, A. M. Elshahawy, D. Zhao, S. J. Pennycook, J. Wang, *ACS Energy Lett.* **2018**, *3*, 2462.
- [148] X. Han, Y. Yang, J. J. Zhou, Q. Ma, K. Tao, L. Han, *Chemistry* **2018**, *24*, 18106.
- [149] J. Li, Y. Deng, L. Leng, M. Liu, L. Huang, X. Tian, H. Song, X. Lu, S. Liao, *J. Power Sources* **2020**, *450*, 227725.
- [150] H. Chen, Z. Shen, Z. Pan, Z. Kou, X. Liu, H. Zhang, Q. Gu, C. Guan, *J. Wang, Adv. Sci.* **2019**, *6*, 1802002.
- [151] X. Liu, L. Zhang, X. Gao, C. Guan, Y. Hu, J. Wang, *ACS Appl. Mater. Interfaces* **2019**, *11*, 23236.
- [152] X. Zhu, Y. Wu, Y. Lu, Y. Sun, Q. Wu, Y. Pang, Z. Shen, H. Chen, *J. Colloid Interface Sci.* **2021**, *587*, 693.
- [153] Y. Tao, Y. Wu, H. Chen, W. Chen, J. Wang, Y. Tong, G. Pei, Z. Shen, C. Guan, *Chem. Eng. J.* **2020**, *396*, 125364.
- [154] Y. Zhang, H. Chen, C. Guan, Y. Wu, C. Yang, Z. Shen, Q. Zou, *ACS Appl. Mater. Interfaces* **2018**, *10*, 18440.

- [155] X. Liu, C. Guan, Y. Hu, L. Zhang, A. M. Elshahawy, J. Wang, *Small* **2018**, *14*, 1702641.
- [156] D. Cai, J. Du, C. Zhu, Q. Cao, L. Huang, J. Wu, D. Zhou, Q. Xia, T. Chen, C. Guan, Y. Xia, *ACS Appl. Energy Mater.* **2020**, *3*, 12162.
- [157] Z. Peng, J. Huang, Y. Wang, K. Yuan, L. Tan, Y. Chen, *J. Mater. Chem. A* **2019**, *7*, 27313.
- [158] W. Chen, T. Wei, L.-E. Mo, S. Wu, Z. Li, S. Chen, X. Zhang, L. Hu, *Chem. Eng. J.* **2020**, *400*, 125856.
- [159] S. Tan, Z. Xue, K. Tao, L. Han, *Chem. Commun.* **2022**, *58*, 6243.
- [160] Y. Tian, Z. Xue, Q. Zhao, J. Guo, K. Tao, L. Han, *Dalton Trans.* **2022**, *51*, 4406.
- [161] X. Xia, C. Zhu, J. Luo, Z. Zeng, C. Guan, C. F. Ng, H. Zhang, H. J. Fan, *Small* **2014**, *10*, 766.
- [162] W. Zhang, X. Zhao, Y. Zhao, J. Zhang, X. Li, L. Fang, L. Li, *ACS Appl. Mater. Interfaces* **2020**, *12*, 10280.
- [163] W. Zhao, Y. Zheng, L. Cui, D. Jia, D. Wei, R. Zheng, C. Barrow, W. Yang, J. Liu, *Chem. Eng. J.* **2019**, *371*, 461.
- [164] Z. Liu, Y. Qiu, A. Zhang, W. Yang, C. J. Barrow, J. M. Razal, J. Liu, *J. Mater. Chem. A* **2021**, *9*, 22573.
- [165] H. Chen, M. Q. Wang, Y. Yu, H. Liu, S. Y. Lu, S. J. Bao, M. Xu, *ACS Appl. Mater. Interfaces* **2017**, *9*, 35040.
- [166] Q. Cheng, C. Yang, K. Tao, L. Han, *Electrochim. Acta* **2020**, *341*, 136042.
- [167] A. Bahaa, J. Balamurugan, N. H. Kim, J. H. Lee, *J. Mater. Chem. A* **2019**, *7*, 8620.
- [168] J. Cai, Y. Song, X. Chen, Z. Sun, Y. Yi, J. Sun, Q. Zhang, *J. Mater. Chem. A* **2020**, *8*, 1757.
- [169] H. Zhang, Z. Zhao, Y.-N. Hou, Y. Tang, J. Liang, X. Liu, Z. Zhang, X. Wang, J. Qiu, *J. Mater. Chem. A* **2019**, *7*, 9230.
- [170] Y. Huang, L. Quan, T. Liu, Q. Chen, D. Cai, H. Zhan, *Nanoscale* **2018**, *10*, 14171.
- [171] S. Li, M. Hua, Y. Yang, X. Zheng, W. Huang, P. Si, L. Ci, J. Lou, *Sci. China Mater.* **2021**, *64*, 2439.
- [172] Q. Yang, Q. Wang, Y. Long, F. Wang, L. Wu, J. Pan, J. Han, Y. Lei, W. Shi, S. Song, *Adv. Energy Mater.* **2020**, *10*, 1903193.
- [173] Q. Yang, Y. Liu, M. Yan, Y. Lei, W. Shi, *Chem. Eng. J.* **2019**, *370*, 666.
- [174] Q. Yang, Y. Liu, C. Deng, M. Yan, W. Shi, *J. Mater. Chem. A* **2019**, *7*, 26131.
- [175] X. X. Liu, Q. He, Y. Wang, J. Wang, Y. Xiang, D. J. Blackwood, R. Wu, J. S. Chen, *Electrochim. Acta* **2020**, *346*, 136201.
- [176] D. Wang, L. Tian, J. Huang, D. Li, J. Liu, Y. Xu, H. Ke, Q. Wei, *Electrochim. Acta* **2020**, *334*, 135636.
- [177] W. Ren, H. Zhang, C. Guan, C. Cheng, *Green Energy Environ.* **2018**, *3*, 42.
- [178] Y. Wang, J. Huang, Y. Xiao, Z. Peng, K. Yuan, L. Tan, Y. Chen, *Carbon* **2019**, *147*, 146.
- [179] S. Liu, D. Gao, J. Li, K. S. Hui, Y. Yin, K. N. Hui, S. Chan Jun, *J. Mater. Chem. A* **2019**, *7*, 26618.
- [180] M. S. Javed, H. Lei, J. Li, Z. Wang, W. Mai, *J. Mater. Chem. A* **2019**, *7*, 17435.
- [181] W. Ren, H. Zhang, C. Guan, C. Cheng, *Adv. Funct. Mater.* **2017**, *27*, 1702116.
- [182] T. Chen, S. Li, J. Wen, P. Gui, Y. Guo, C. Guan, J. Liu, G. Fang, *Small* **2018**, *14*, 1700979.
- [183] Z. Qian, Y. Chen, Z. Tang, Z. Liu, X. Wang, Y. Tian, W. Gao, *Nano-Micro Lett.* **2019**, *11*, 28.
- [184] X. Li, H. Wu, C. Guan, A. M. Elshahawy, Y. Dong, S. J. Pennycook, J. Wang, *Small* **2019**, *15*, 1803895.
- [185] Z. Chen, Y. Yang, Z. Ma, T. Zhu, L. Liu, J. Zheng, X. Gong, *Adv. Funct. Mater.* **2019**, *29*, 1904182.
- [186] T. T. Nguyen, J. Balamurugan, V. Aravindan, N. H. Kim, J. H. Lee, *Chem. Mater.* **2019**, *31*, 4490.
- [187] J. Lin, H. Wang, Y. Yan, X. Zheng, H. Jia, J. Qi, J. Cao, J. Tu, W. Fei, J. Feng, *J. Mater. Chem. A* **2018**, *6*, 19151.
- [188] J. Liu, J. Liang, C. Wang, J. Ma, *J. Energy Chem.* **2019**, *33*, 160.
- [189] X. Li, W. Zhang, Y. Feng, W. Li, P. Peng, J. Yao, M. Li, C. Jiang, *Electrochim. Acta* **2019**, *294*, 173.
- [190] Z. Li, L. Y. Zhang, L. Zhang, J. Huang, H. Liu, *Nanoscale Res. Lett.* **2019**, *14*, 358.
- [191] C. Zhu, C. Guan, D. Cai, T. Chen, Y. Wang, J. Du, J. Wu, X. Xu, H. Yu, W. Huang, *Batteries Supercaps* **2020**, *3*, 93.
- [192] H. Zhang, T. Wang, A. Sumboja, W. Zang, J. Xie, D. Gao, S. J. Pennycook, Z. Liu, C. Guan, J. Wang, *Adv. Funct. Mater.* **2018**, *28*, 1804846.
- [193] Y. Xie, J. Cao, X. Wang, W. Li, L. Deng, S. Ma, H. Zhang, C. Guan, W. Huang, *Nano Lett.* **2021**, *21*, 8579.
- [194] Y. Tang, X. Li, H. Lv, D. Xie, W. Wang, C. Zhi, H. Li, *Adv. Energy Mater.* **2020**, *10*, 2000892.
- [195] K. R. Yoon, K. Shin, J. Park, S. H. Cho, C. Kim, J. W. Jung, J. Y. Cheong, H. R. Byon, H. M. Lee, I. D. Kim, *ACS Nano* **2018**, *12*, 128.
- [196] Y. Yao, H. Wang, H. Yang, S. Zeng, R. Xu, F. Liu, P. Shi, Y. Feng, K. Wang, W. Yang, X. Wu, W. Luo, Y. Yu, *Adv. Mater.* **2020**, *32*, 1905658.
- [197] F. Zhan, S. Liu, Q. He, X. Zhao, H. Wang, M. Han, Y. Yamauchi, L. Chen, *Energy Storage Mater.* **2022**, *52*, 685.
- [198] C. Guan, A. Sumboja, W. Zang, Y. Qian, H. Zhang, X. Liu, Z. Liu, D. Zhao, S. J. Pennycook, J. Wang, *Energy Storage Mater.* **2019**, *16*, 243.
- [199] J. Huang, Z. Peng, Y. Xiao, Y. Xu, L. Chen, Y. Xiong, L. Tan, K. Yuan, Y. Chen, *Adv. Sci.* **2019**, *6*, 1900550.
- [200] Q. Xu, H. Jiang, Y. Li, D. Liang, Y. Hu, C. Li, *Appl. Catal. B: Environ.* **2019**, *256*, 117893.
- [201] E. Hu, J. Ning, D. Zhao, C. Xu, Y. Lin, Y. Zhong, Z. Zhang, Y. Wang, Y. Hu, *Small* **2018**, *14*, 1704233.
- [202] H. Zhang, W. Tian, X. Duan, H. Sun, S. Liu, S. Wang, *Adv. Mater.* **2020**, *32*, 1904037.
- [203] Y. Chen, S. Ji, C. Chen, Q. Peng, D. Wang, Y. Li, *Joule* **2018**, *2*, 1242.
- [204] J. Gu, C.-S. Hsu, L. Bai, H. M. Chen, X. Hu, *Science* **2019**, *364*, 1091.
- [205] W. Zang, A. Sumboja, Y. Ma, H. Zhang, Y. Wu, S. Wu, H. Wu, Z. Liu, C. Guan, J. Wang, S. J. Pennycook, *ACS Catal.* **2018**, *8*, 8961.
- [206] L. Huang, W. Zang, Y. Ma, C. Zhu, D. Cai, H. Zhang, H. Yu, Q. Zou, L. Wu, C. Guan, *Chem. Eng. J.* **2021**, *421*, 129973.
- [207] Z. Lian, Y. Lu, C. Wang, X. Zhu, S. Ma, Z. Li, Q. Liu, S. Zang, *Adv. Sci.* **2021**, *8*, 2102550.
- [208] A. Agarwal, B. R. Sankapal, *J. Mater. Chem. A* **2021**, *9*, 20241.
- [209] P. Sun, L. Wang, J. Zhang, J. Huang, P. Wang, J. Hou, J. Zhang, C. Li, Z. Yao, Y. Yang, J. Xiong, *Electrochim. Acta* **2020**, *363*, 137262.
- [210] A. M. Elshahawy, C. Guan, X. Li, H. Zhang, Y. Hu, H. Wu, S. J. Pennycook, J. Wang, *Nano Energy* **2017**, *39*, 162.
- [211] J. Hu, Y. Qin, H. Sun, Y. Ma, L. Lin, Y. Peng, J. Zhong, M. Chen, X. Zhao, Z. Deng, *Small* **2022**, *18*, 2106260.
- [212] L. Quan, S. Li, Z. Zhao, J. Liu, Y. Ran, J. Cui, W. Lin, X. Yu, L. Wang, Y. Zhang, J. Ye, *Small Methods* **2021**, *5*, 2100125.
- [213] K. Xiao, Z. Chen, Z. Liu, L. Zhang, X. Cai, C. Song, Z. Fan, X. Chen, J. Liu, Z. X. Shen, *J. Power Sources* **2020**, *455*, 227959.
- [214] D. Ren, J. Ying, M. Xiao, Y. P. Deng, J. Ou, J. Zhu, G. Liu, Y. Pei, S. Li, A. M. Jauhar, H. Jin, S. Wang, D. Su, A. Yu, Z. Chen, *Adv. Funct. Mater.* **2019**, *30*, 1908167.
- [215] Z. Wang, J. Shen, J. Liu, X. Xu, Z. Liu, R. Hu, L. Yang, Y. Feng, J. Liu, Z. Shi, L. Ouyang, Y. Yu, M. Zhu, *Adv. Mater.* **2019**, *31*, 1902228.
- [216] Q. Zhang, Z. Zhou, Z. Pan, J. Sun, B. He, Q. Li, T. Zhang, J. Zhao, L. Tang, Z. Zhang, L. Wei, Y. Yao, *Adv. Sci.* **2018**, *5*, 1801462.
- [217] J. Jin, W. Cai, J. Cai, Y. Shao, Y. Song, Z. Xia, Q. Zhang, J. Sun, *J. Mater. Chem. A* **2020**, *8*, 3027.
- [218] Y. Pan, Y. Zhao, S. Mu, Y. Wang, C. Jiang, Q. Liu, Q. Fang, M. Xue, S. Qiu, *J. Mater. Chem. A* **2017**, *5*, 9544.
- [219] Z. Li, L. Yin, *Nanoscale* **2015**, *7*, 9597.

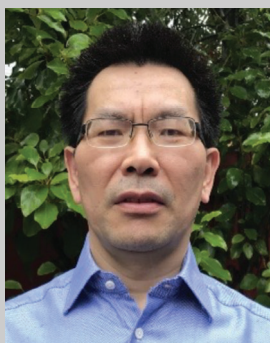
- [220] L. Kong, J. Zhu, W. Shuang, X.-H. Bu, *Adv. Energy Mater.* **2018**, *8*, 1801515.
- [221] Y. Li, J. Cao, L. Wang, Y. Qiao, Y. Zhou, H. Xie, J. Li, *J. Energy Storage* **2022**, *55*, 105485.
- [222] K. Chen, Z. Sun, R. Fang, Y. Shi, H.-M. Cheng, F. Li, *Adv. Funct. Mater.* **2018**, *28*, 1870274.
- [223] L. Niu, T. Z. Wu, M. Chen, L. Yang, J. J. Yang, Z. X. Wang, A. A. Kornyshev, H. L. Jiang, S. Bi, G. Feng, *Adv. Mater.* **2022**, *34*, 17.
- [224] B. J. Zhu, D. S. Wen, Z. B. Liang, R. Q. Zou, *Coord. Chem. Rev.* **2021**, *446*, 21.
- [225] L. S. Xie, G. Skorupskii, M. Dinca, *Chem. Rev.* **2020**, *120*, 8536.



Dongming Cai received both his BSc and PhD from Hubei University, China in 2017 and 2022 respectively. Then he joined School of Mathematics, Physics and Optoelectronics Engineering at Hubei University of Automotive Technology. His current research is focused on the design and synthesis of novel nanostructured materials and their applications in electrochemical energy storage and conversion field, including Zn-ion batteries, supercapacitors, and electrocatalytic water splitting etc.



Zhuxian Yang received her BSc from East China Normal University in 1995 and her MSc from Fudan University, China in 1998. She earned her PhD in 2007 from the School of Chemistry at the University of Nottingham in the United Kingdom, working on the synthesis, characterization, and application of micro/mesoporous carbon materials. She is now a Research Fellow in the College of Engineering, Mathematics and Physics Sciences, University of Exeter, working on the conversion of carbon dioxide to dimethyl carbonate. Her research interests include applications of porous materials in gas storage and separation, as catalysts and electrocatalysts.



Yongde Xia earned his PhD from Fudan University, China. After postdoctoral experience in Korea and France, he moved to UK and worked as a Research Fellow at the University of Nottingham. Followed by joining Exeter in 2010, he is now a Senior Lecturer in Functional Materials in the College of Engineering, Mathematics and Physics Sciences at University of Exeter. His main research interests include novel porous materials for energy, electrochemical energy storage and conversion, photocatalysis and adsorption. He contributes to over 170 peer-reviewed journal publications.